[redacted]

Copy 37
RM SL55J26

[redacted]

NACA

RESEARCH MEMORANDUM

for the

U. S. Army Chemical Corps

WIND-TUNNEL INVESTIGATION AT LOW SPEED OF THE AERODYNAMIC CHARACTERISTICS OF THE ARMY CHEMICAL CORPS MODEL E112 BOMBLETS

By William Letko and James L. Williams

Langley Aeronautical Laboratory
Langley Field, Va.

[redacted]

NATIONAL ADVISORY COMMITTEE
FOR AERONAUTICS

WASHINGTON
NOV 4 1955

[redacted]

NATIONAL ADVISORY COMMITTEE FOR AERONAUTICS

RESEARCH MEMORANDUM

for the

U. S. Army Chemical Corps

WIND-TUNNEL INVESTIGATION AT LOW SPEED OF THE AERODYNAMIC CHARACTERISTICS OF THE ARMY CHEMICAL CORPS MODEL E112 BOMBLETS

By William Letko and James L. Williams

SUMMARY

An experimental investigation has been made in the Langley stability tunnel to determine the aerodynamic characteristics of the Army Chemical Corps model E112 bomblets. A detailed analysis has not been made; however, the results showed that a gap between model tips and the end plates or increasing the end-plate size for a solid model could result in a spirally stable configuration.

INTRODUCTION

At the request of the U. S. Army Chemical Corps, a low-speed wind-tunnel investigation of the Cook Research Laboratories vortex gliders (designated as the Army Chemical Corps model E112 bomblets) was made in the Langley stability tunnel. The vortex glider or bomblet was designed for use in certain military applications where dispersal of small units over very large areas is desirable. The vortex glider under consideration was designed to rotate rapidly about its spanwise axis while falling. This rotation induces a circulation about the glider; consequently, a lift is produced. Lift-drag ratios from 1.0 to 2.0 are practicably achievable and are high enough to be of military value. The advantage of this glider over conventional wing-alone or wing-body gliders arises as a result of the rapid lift-producing rotation which introduces a gyroscopic stiffness that assists in preserving the initial heading. Drop tests by Cook Research Laboratories of several configurations of the vortex glider, however, showed that the gliders were spirally unstable.

The tests of this investigation were made to aid in the development of the vortex glider, particularly, to determine a spirally stable configuration. Static and dynamic lateral stability derivatives were determined for the original models and for the models as modified during the course of the investigation. In order to expedite distribution of the results of this investigation, a detailed analysis has not been made.

SYMBOLS

The data are presented about the stability axes and positive direction of forces and moments are shown in figure 1. The coefficients and symbols used are defined as follows:

C_L lift coefficient, L/qS

C_D drag coefficient, D/qS

C_Y lateral-force coefficient, F_Y/qS

C_l rolling-moment coefficient, M_X/qSb

C_n yawing-moment coefficient, M_Z/qSb

L lift

D drag

F_Y lateral force

M_X rolling moment

M_Z yawing moment

q dynamic pressure

I_X moment of inertia coefficient about X-axis, $2\left(\frac{k_X}{b}\right)^2$

I_Y moment of inertia coefficient about Y-axis, $\frac{2\mu b}{c}\eta\left(\frac{k_Y}{b}\right)^2$

k_X radius of gyration about X-axis

[redacted]

k_Y radius of gyration about Y-axis

$$\mu = \frac{m}{\rho S b}$$

m mass

ρ mass density of air

b span

c chord

S area

$$\eta = \frac{2\pi n c}{V}$$

n rotational speed of model, revolutions per sec

V free-stream velocity

r yawing angular velocity

p rolling angular velocity

$\frac{rb}{2V}$ yawing-velocity parameter

$\frac{pb}{2V}$ rolling-velocity parameter

β angle of sideslip

γ glide path angle, positive in climb

$$C_{Y_\beta} = \frac{\partial C_Y}{\partial \beta}$$

$$C_{l_\beta} = \frac{\partial C_l}{\partial \beta}$$

[redacted]

$$C_{n_\beta} = \frac{\partial C_n}{\partial \beta}$$

$$C_{Y_r} = \frac{\partial C_Y}{\partial \frac{rb}{2V}}$$

$$C_{l_r} = \frac{\partial C_l}{\partial \frac{rb}{2V}}$$

$$C_{n_r} = \frac{\partial C_n}{\partial \frac{rb}{2V}}$$

$$C_{Y_p} = \frac{\partial C_Y}{\partial \frac{pb}{2V}}$$

$$C_{l_p} = \frac{\partial C_l}{\partial \frac{pb}{2V}}$$

$$C_{n_p} = \frac{\partial C_n}{\partial \frac{pb}{2V}}$$

APPARATUS AND MODELS

All tests were made in the Langley stability tunnel. The static yawing and stability derivatives were obtained in the 6- by 6-foot curved-flow test section in which curved flight is simulated by causing air to flow in a curved path about a fixed model. The rolling derivatives were obtained in the 6-foot-diameter test section in which rolling flight is simulated by twisting the air about a fixed model.

Three models were supplied by Cook Research Laboratories (see fig. 2). Models 1 and 2 were mainly made of mahogany with metal end plates. Model 3 was made of magnesium and provision was made for changing the end plates.

Removable tip blocks were supplied with model 3 so that tests could be made with different gaps between end plates and model tips. The geometric characteristics of the models are given in figure 3. The dimensions of different end plates tested with model 3 are given in figure 4. A 3/4-inch shaft mounted in ball bearings passed through each model and was fastened to a yoke support (fig. 2(b)) which in turn was mounted on a six-component mechanical balance system. During the tests the models were free to rotate about the shaft and the rotational speed was measured with a Strobotac. As a matter of interest it should be pointed out that the tunnel models were about three times the size of a practical flight model.

CORRECTIONS

No jet boundary corrections have been applied to the data. Support strut tare corrections, however, have been applied and the lateral-force coefficient has been corrected for the buoyancy effect of the static-pressure gradient associated with curved flow.

TESTS

Tests of models 1 and 2 were made at a dynamic pressure of 8 and 16 pounds per square foot. All tests of model 3 were made at a dynamic pressure of 8 pounds per square foot. The airspeeds and Reynolds number (based on chord) for the models are given in the following table.

Model	q	V, ft/sec	Reynolds number
1	8	84	400,000
1	16	117	553,000
2	8	84	620,000
2	16	117	866,000
3	8	84	436,000

PRESENTATION OF RESULTS

The results of the investigation are presented in figures 5 to 48. All data presented for models 1, 2, and 3 are based on the following geometric characteristics.

[redacted]

Model	Chord, ft	Span, ft	Area, sq ft
1	0.750	2.500	1.875
2	1.167	2.500	2.916
3	.817	2.492	2.036

The values of C_{n_β}, C_{l_β}, and C_{Y_β} presented in table 1 are the slopes of the coefficients against β obtained near $\beta = 0$.

The derivatives C_{n_r}, C_{l_r}, C_{Y_r}, C_{n_p}, C_{l_p}, and C_{Y_p} presented for β other than zero were obtained from plots of the coefficients against $rb/2V$ and $pb/2V$ similar to those presented for $\beta = 0$. Table 2 is provided as an index to the figures.

DISCUSSION

In order to determine which of the stability derivatives are important for dynamic stability of the vortex glider a study of the coefficients of the roots of the stability quartic for the vortex glider is necessary. It is well known that the necessary and sufficient conditions for stability are that the real parts of the roots of the stability quartic be negative. In order that the real parts of the roots shall all be negative, it is necessary that B, C, D, E and $(BCD-D^2-B^2D)$ each be positive. The equations for these coefficients have been determined for the vortex glider by Mr. R. A. Fredette of Cook Laboratories in an unpublished report titled, "Dynamic Stability of Vortex Gliders." Since the original models were spirally unstable and since the algebraic sign of the coefficient E determines spiral stability or instability, the coefficient E was examined to determine which of its terms was of most importance. The study showed that the expression for E is similar to that for normal airplane configurations and that for the vortex glider the derivatives C_{l_β} and C_{n_β} are predominant in determining whether E is positive or negative. The study also showed that the dynamic stability derivatives which are found in the expression for E could be neglected without altering the conclusions with regard to spiral stability. This resulted in the following approximate expression for E

$$E = k\left(C_{l_\beta} \sin \gamma - C_{n_\beta} \cos \gamma\right)$$

where k is composed of spin ratio, lift, mass and inertia terms. Equating $E = 0$ to determine the spiral stability boundary eliminates k and results in the following expression

$$C_{l_\beta} \tan \gamma = C_{n_\beta}$$

and

$$\frac{C_{n_\beta}}{C_{l_\beta}} = \tan \gamma = -\frac{D}{L}$$

The slope of the spiral stability boundary is, therefore, the negative reciprocal of the lift-drag ratio. The approximate $E = 0$ boundary provided a simple criterion for determining whether a configuration was spirally stable or unstable and whether the modifications tried were beneficial or not.

The values of C_{n_β} and C_{l_β} obtained for model 1 indicate a spirally unstable configuration as can be seen in figure 45. The values of C_{n_β} and C_{l_β} fell in the unstable region as defined by the $E = 0$ boundary. This configuration was one of the configurations tested in flight and found to be spirally unstable. Although the values of C_{n_β} and C_{l_β} obtained for model 2 indicate a spirally stable model at $q = 16$ as can be seen in figure 46, the values for $q = 8$ indicate spiral instability although this is not shown on the figure. Most of the configurations tested were found to have values of C_{n_β} and C_{l_β} such that an unstable configuration resulted. However, it was found that a gap between the model tip and the end plate would result in stability for some of the configurations tested. This is shown in figure 47. The D/L ratio for the configurations indicated on the figure varies only from 0.91 to 1.05 so that for simplicity an average boundary was drawn. The configurations shown fall well into the stable region. These configurations however have a lower L/D ratio than the solid models. This ratio is between 0.95 and 1.20 for models with a gap. See table 1.

A spirally stable configuration also resulted for a model with very large end plates (end plates number 6, see fig. 4(b)). The boundaries for this model both with and without a gap are shown on figure 48 and both configurations are seen to fall into the stable region. The

[redacted]

L/D ratio for the solid model is seen from table 1 to be 2.17 while the L/D ratio for the model with $2\frac{7}{16}$-inch gap is 0.95.

The inertia of the model with large end plates is probably high and the inertia of the actual flight model would also probably be relatively high and would require a longer time before full rotation and final glide path angle is reached.

CONCLUDING REMARKS

The results of the investigation show that a gap between model tips and end plates makes some configurations spirally stable, although the lift-drag ratio is decreased from that for a solid model. Large area end plates (19-inch diameter) result in spiral stability even for a solid model with a lift-drag ratio of about 2.0.

Langley Aeronautical Laboratory,
National Advisory Committee for Aeronautics,
Langley Field, Va., October 13, 1955.

William Letko
William Letko
Aeronautical Research Scientist

James L. Williams
James L. Williams
Aeronautical Research Scientist

Approved: Thomas A. Harris
Thomas A. Harris
Chief of Stability Research Division

DY

[redacted]

TABLE 1.- GEOMETRIC AND AERODYNAMIC CHARACTERISTICS OF MODELS

Model	q	Driving vane	Gap size	End plate	[a] I_X	[a] I_Y	[a] μ	$\frac{2\pi nc}{V}$	$\frac{L}{D}$	C_L	C_D	[b] C_{n_β}	[b] C_{l_β}	[b] C_{Y_β}	C_{n_p}	C_{l_r}	C_{Y_r}	C_{n_p}	C_{l_p}	C_{Y_p}
1	8	On	0	See figure 3				2.26	1.43	2.49	1.74	0.0032	-0.0010	-0.0195				-0.260	-0.260	0.310
1	16		0					2.28	1.48	2.52	1.71	.0039	-.0016	-.0185				-.290	-.265	.310
2	8		0					2.43	1.39	2.40	1.73	.0008	-.0006	-.0255	-0.500	0.205	0.220	-.200	-.245	.505
2	16		0					2.46	1.38	2.33	1.69	.0008	-.0013	-.0255	-.305	.180	.090	-.235	-.280	.555
3	8		0	1				2.44	1.62	2.55	1.57	.0034	.0018	-.0174	-.355	.331	.208			
3			$\frac{5}{8}$	1				1.75	1.21	1.56	1.29	.0035	-.0016	-.0235						
3			$1\frac{7}{32}$	1				1.68	1.07	1.35	1.25	.0032	-.0006	-.0270						
3			$2\frac{7}{16}$	1				1.53	.95	1.13	1.18	.0018	-.0009	-.0280	-.265	.031	.090			
3			0	2				2.41	1.66	2.61	1.57	.0033	.0010	-.0163						
3			$2\frac{7}{16}$	2				1.58	.93	1.13	1.22	.0017	-.0005	-.0292						
3			0	[c] 3				2.30	1.65	2.38	1.44	.0019	.0059	-.0415						
3			$2\frac{7}{16}$	[c] 3				1.55	.96	1.10	1.15	-.0004	-.0004	-.0465	-.496	.112	.574			
3			0	[d] 3				2.32	1.90	2.70	1.42	.0035	.0005	-.0434						
3			$2\frac{7}{16}$	[d] 3				1.54	.96	1.10	1.14	-.0007	-.0069	-.0434						
3			0	4				2.81	1.65	2.91	1.76	.0100	-.0127	-.0291	-.241	.380	.306			
3			$2\frac{7}{16}$	4				1.64	.98	1.11	1.13	.0017	-.0009	-.0212	-.402	.131	.396			
3			0	5				2.67	1.97	3.28	1.66	.0015	-.0016	-.0395	-.441	.265	.329			
3			$2\frac{7}{16}$	5				1.61	.98	1.12	1.15	-.0006	-.0009	-.0422	-.361	.131	.453			
3			0	6	0.2425	54.30	201	2.36	2.17	2.84	1.31	-.0021	-.0012	-.0667	-.735	.476	1.098			
3			$2\frac{7}{16}$	6	.2030	32.25	198	1.51	.95	1.09	1.14	-.0058	-.0009	-.0715	-.537	.149	1.094			
3			0	7				1.54	1.20	1.43	1.19	.0062	.0020	-.0136						
3			$2\frac{7}{16}$	7				1.50	.94	1.03	1.10	.0039	.0025	-.0151						
3		Off	$2\frac{7}{16}$	1				1.47	1.10	1.15	1.05	-.0012	-.0010	-.0268						
3		On	0	Off				1.70	1.13	1.43	1.27	.0059	-.0013	.0044						
3		On	[e] $2\frac{7}{16}$	Off				1.63	.95	1.08	1.13	.0040	-.0018	.0078						

[a] Values supplied by Cook Research Laboratories.

[b] Slopes per degree.

[c] Long dimension perpendicular to chord.

[d] Long dimension parallel to chord.

[e] $2\frac{7}{16}$- inch filler blocks removed.

TABLE 2.- INDEX OF FIGURES

Figure	Model	Gap size	End plate	Driving vane	q	Data presented
5	1	0	See figure 3	On	8,16	C_L, C_D, n against β
6	1	0	See figure 3		8,16	C_n, C_l, C_Y against β
7	1	0	See figure 3		8,16	C_n, C_l, C_Y, n against $\frac{pb}{2V}$
8	1	0	See figure 3		8,16	C_{n_p}, C_{l_p}, C_{Y_p} against β
9	2	0	See figure 3		8,16	C_L, C_D, n against β
10	2	0	See figure 3		8,16	C_n, C_l, C_Y against β
11	2	0	See figure 3		8,16	C_n, C_l, C_Y, n against $\frac{rb}{2V}$
12	2	0	See figure 3		8,16	C_n, C_l, C_Y, n against $\frac{pb}{2V}$
13	2	0	See figure 3		8,16	C_{n_r}, C_{l_r}, C_{Y_r} against β
14	2	0	See figure 3		8,16	C_{n_p}, C_{l_p}, C_{Y_p} against β
15	3	0, $\frac{5}{8}$, $1\frac{7}{32}$, $2\frac{7}{16}$	1		8	C_L, C_D, n against β
16	3	0, $\frac{5}{8}$, $1\frac{7}{32}$, $2\frac{7}{16}$	1		8	C_n, C_l, C_Y against β
17	3	0, $2\frac{7}{16}$	1		8	C_n, C_l, C_Y, n against $\frac{rb}{2V}$
18	3	0, $2\frac{7}{16}$	1		8	C_{n_r}, C_{l_r}, C_{Y_r} against β
19	3	0, $2\frac{7}{16}$	2		8	C_L, C_D, n against β
20	3	0, $2\frac{7}{16}$	2		8	C_n, C_l, C_Y against β
21	3	0, $2\frac{7}{16}$	[a] 3		8	C_L, C_D, n against β
22	3	0, $2\frac{7}{16}$	[a] 3		8	C_n, C_l, C_Y against β
23	3	0, $2\frac{7}{16}$	[a] 3		8	C_n, C_l, C_Y, n against $\frac{rb}{2V}$
24	3	0, $2\frac{7}{16}$	[a] 3		8	C_{n_r}, C_{l_r}, C_{Y_r} against β

[a]Long dimension perpendicular to chord.

TABLE 2.- INDEX OF FIGURES - Concluded

Figure	Model	Gap size	End plate	Driving vane	q	Data presented
25	3	0, $2\frac{7}{16}$	[b] 3	On	8	C_L, C_D, n against β
26	3	0, $2\frac{7}{16}$	[b] 3		8	C_n, C_l, C_Y against β
27	3	0, $2\frac{7}{16}$	4		8	C_L, C_D, n against β
28	3	0, $2\frac{7}{16}$	4		8	C_n, C_l, C_Y against β
29	3	0, $2\frac{7}{16}$	4		8	C_n, C_l, C_Y, n against $\frac{rb}{2V}$
30	3	0, $2\frac{7}{16}$	4		8	C_{n_r}, C_{l_r}, C_{Y_r} against β
31	3	0, $2\frac{7}{16}$	5		8	C_L, C_D, n against β
32	3	0, $2\frac{7}{16}$	5		8	C_n, C_l, C_Y against β
33	3	0, $2\frac{7}{16}$	5		8	C_n, C_l, C_Y, n against $\frac{rb}{2V}$
34	3	0, $2\frac{7}{16}$	5		8	C_{n_r}, C_{l_r}, C_{Y_r} against β
35	3	0, $2\frac{7}{16}$	6		8	C_L, C_D, n against β
36	3	0, $2\frac{7}{16}$	6		8	C_n, C_l, C_Y against β
37	3	0, $2\frac{7}{16}$	6		8	C_n, C_l, C_Y, n against $\frac{rb}{2V}$
38	3	0, $2\frac{7}{16}$	6		8	C_{n_r}, C_{l_r}, C_{Y_r} against β
39	3	0, $2\frac{7}{16}$	7		8	C_L, C_D, n against β
40	3	0, $2\frac{7}{16}$	7		8	C_n, C_l, C_Y against β
41	3	$2\frac{7}{16}$	1	Off	8	C_L, C_D, n against β
42	3	$2\frac{7}{16}$	1	Off	8	C_n, C_l, C_Y against β
43	3	0, $2\frac{7}{16}$	Off	On	8	C_L, C_D, n against β
44	3	0, $2\frac{7}{16}$	Off	On	8	C_n, C_l, C_Y against β
45	1	0	See figure 3	On		Spiral stability boundary
46	2	0	See figure 3	On	16	Spiral stability boundary
47	3	0	[a] 3, [b] 3, 5 1	On Off	8	Spiral stability boundary
48	3	0, $2\frac{7}{16}$	6	On	8	Spiral stability boundary

[a] Long dimension perpendicular to chord.

[b] Long dimension parallel to chord.

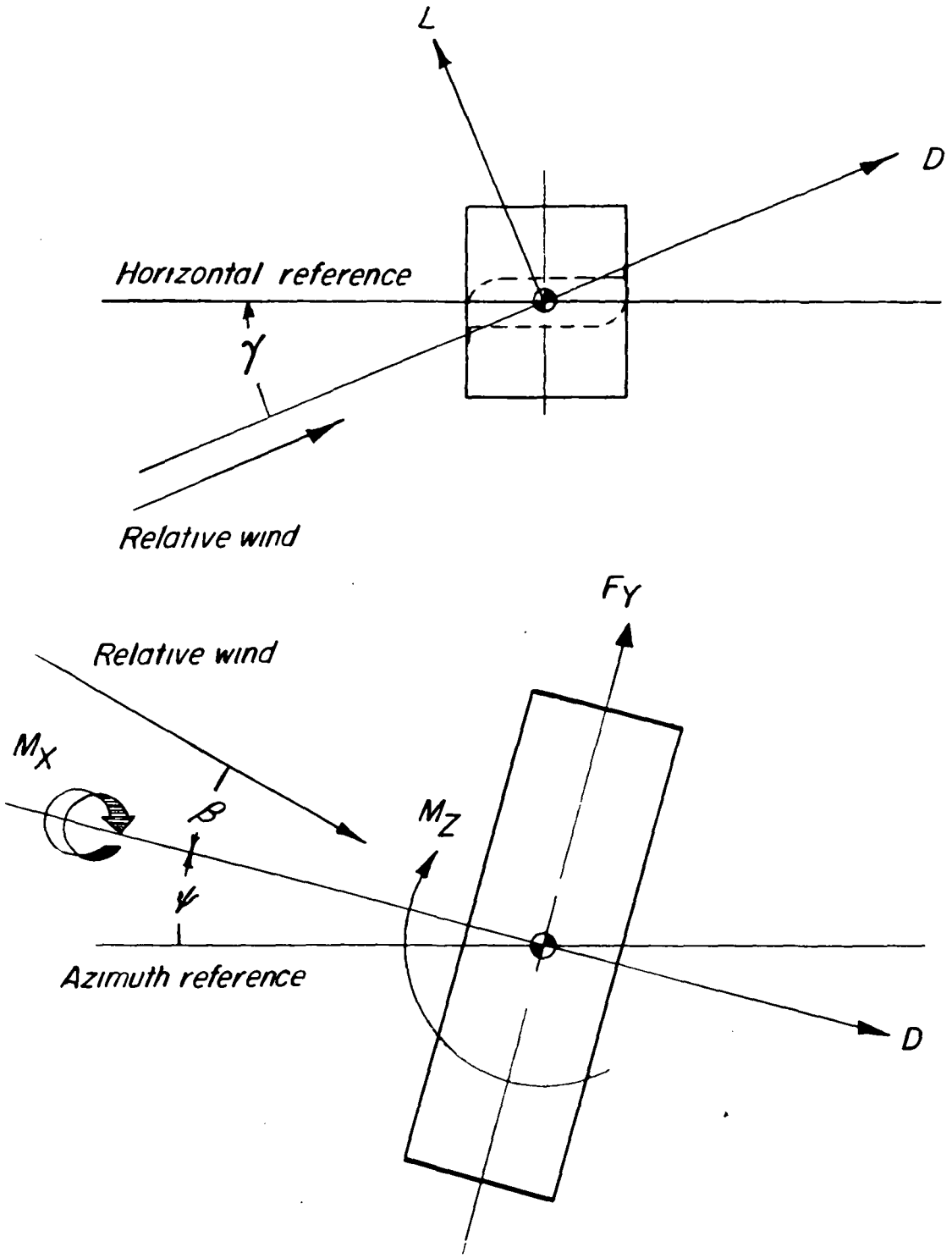

Figure 1.- System of axes used. Arrows indicate positive direction of angles, forces, and moments.

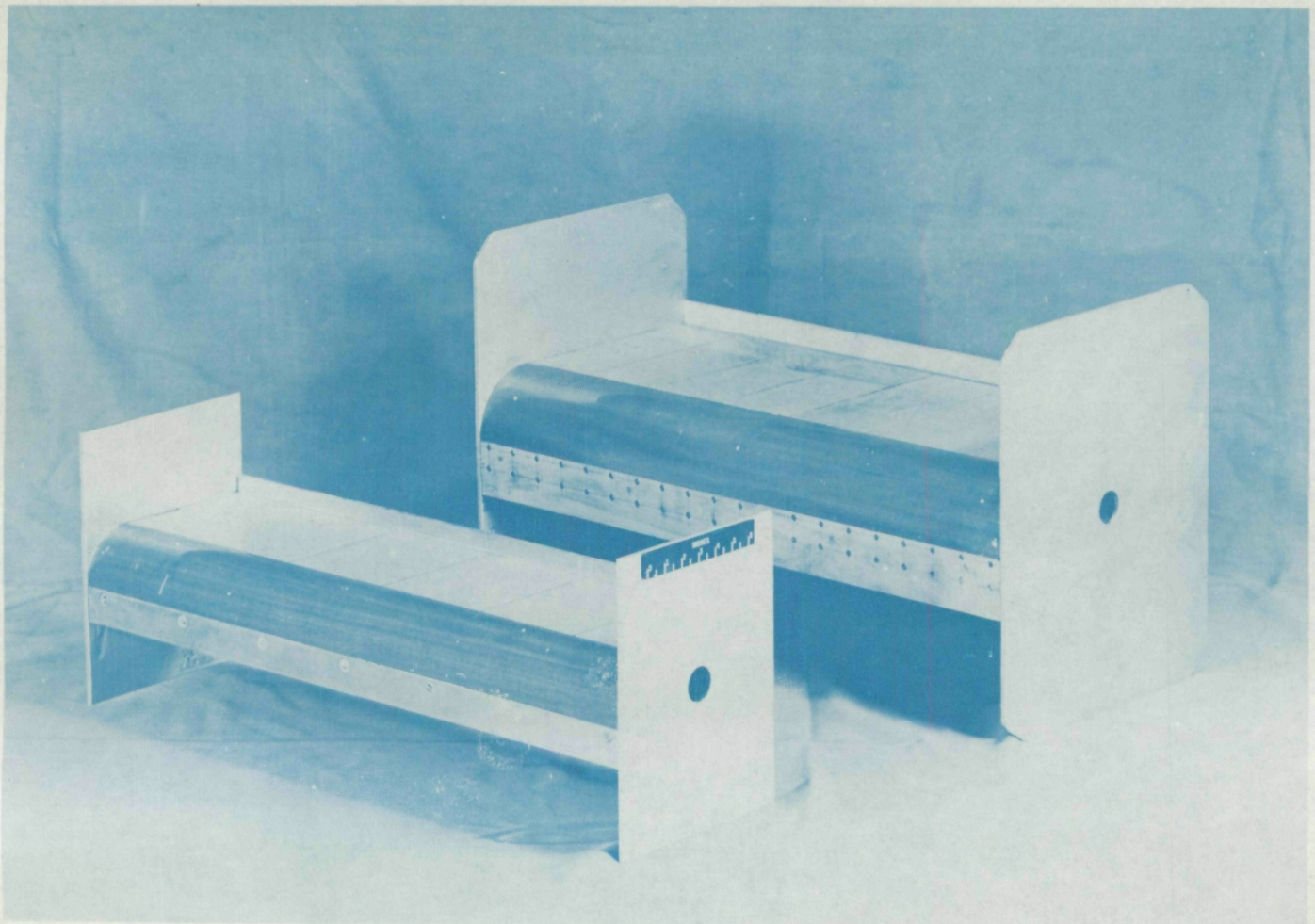

L-88740

(a) Models 1 and 2.

Figure 2.- Photographs of models.

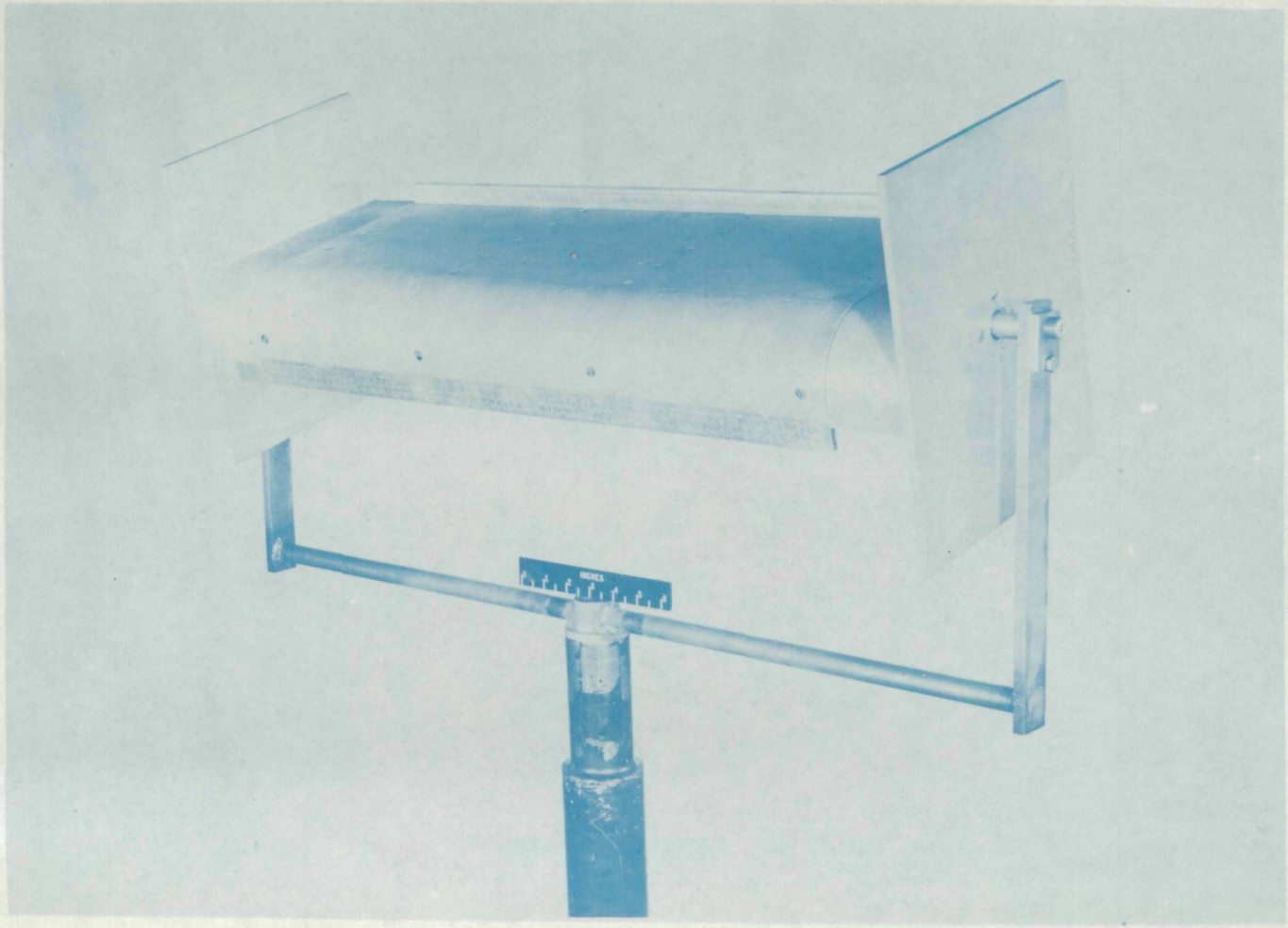

L-90764

(b) Model 3.

Figure 2.- Concluded.

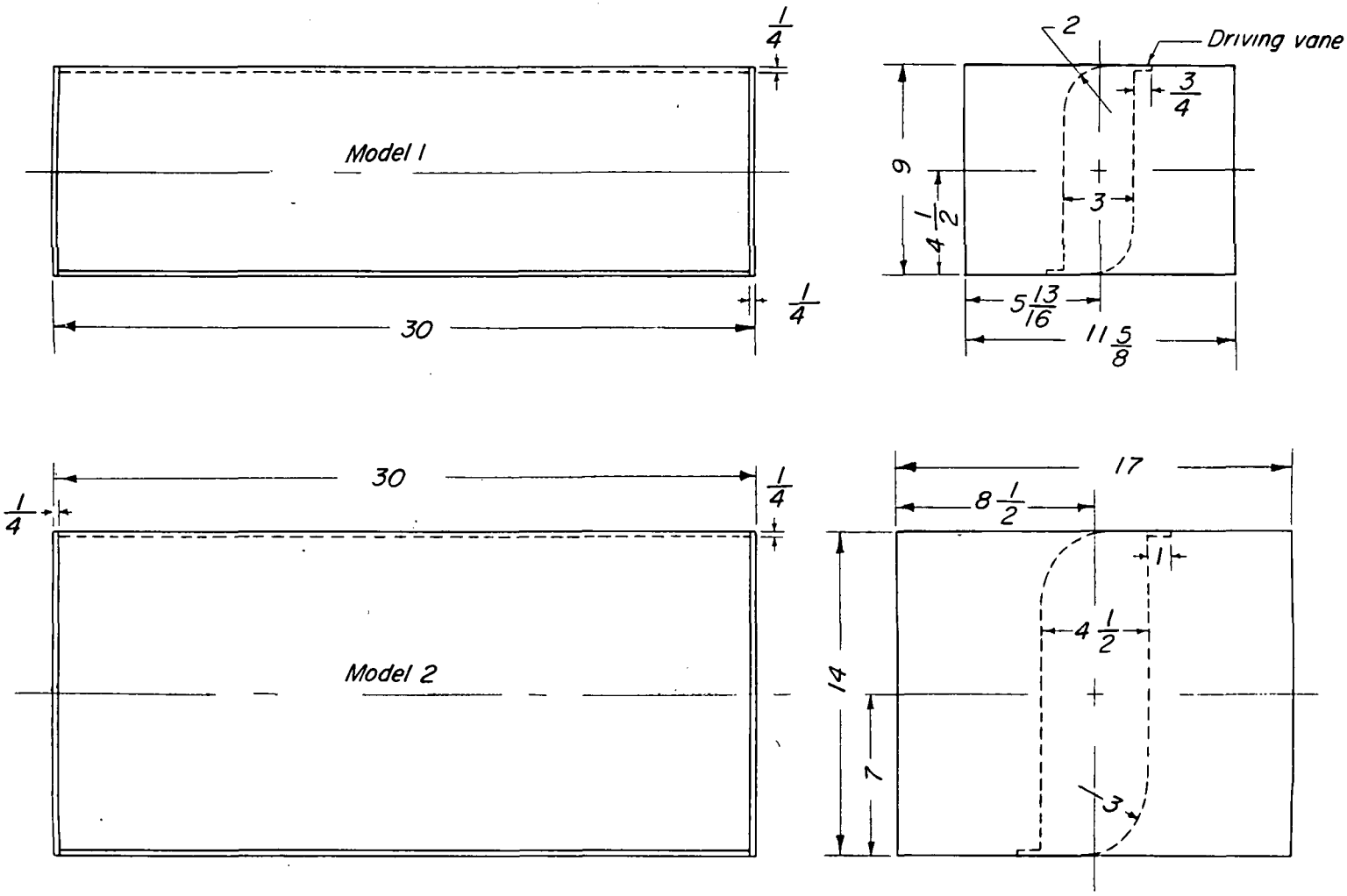

(a) Models 1 and 2.

Figure 3.- Geometric characteristics of models.

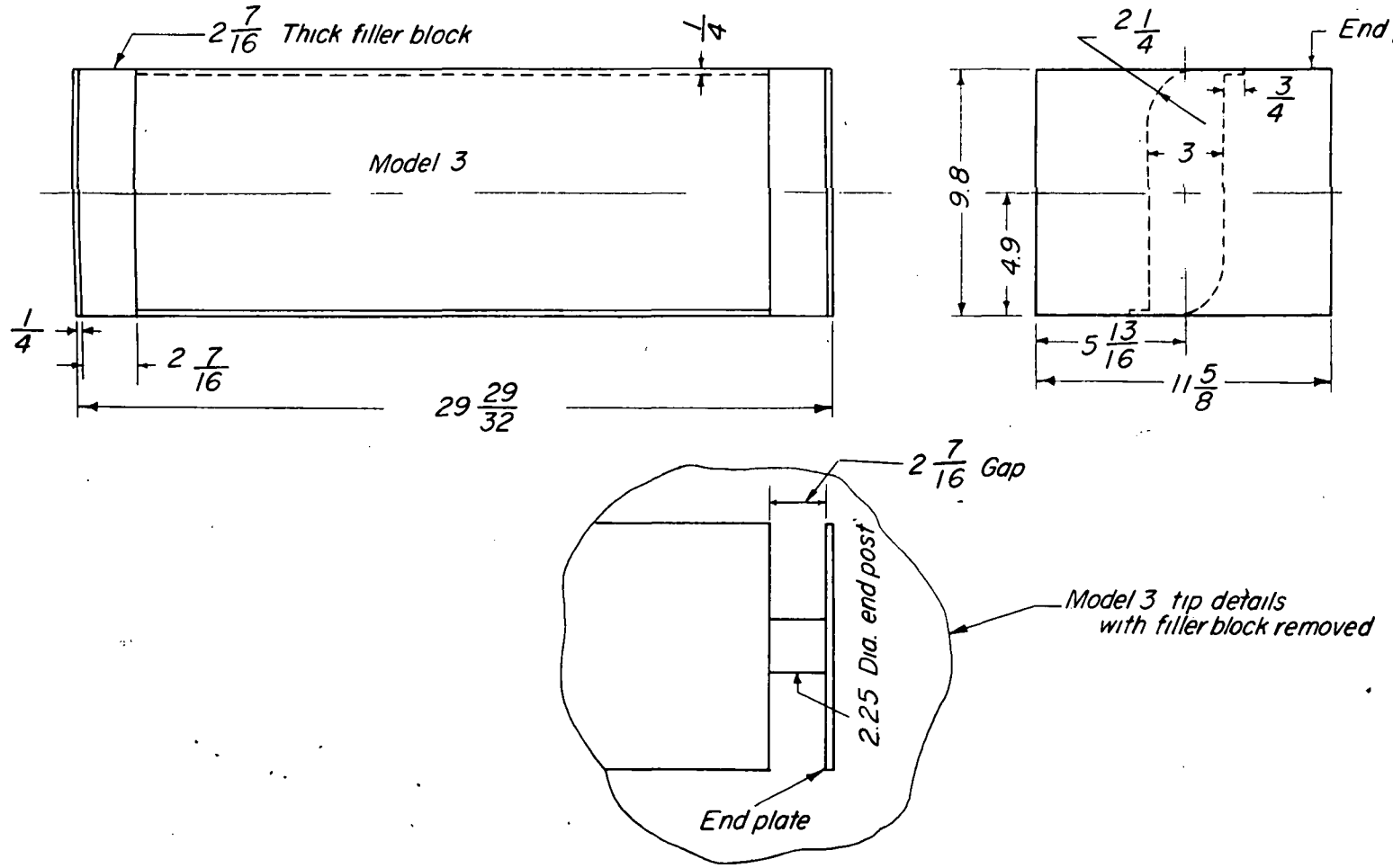

(b) Model 3.

Figure 3.- Concluded.

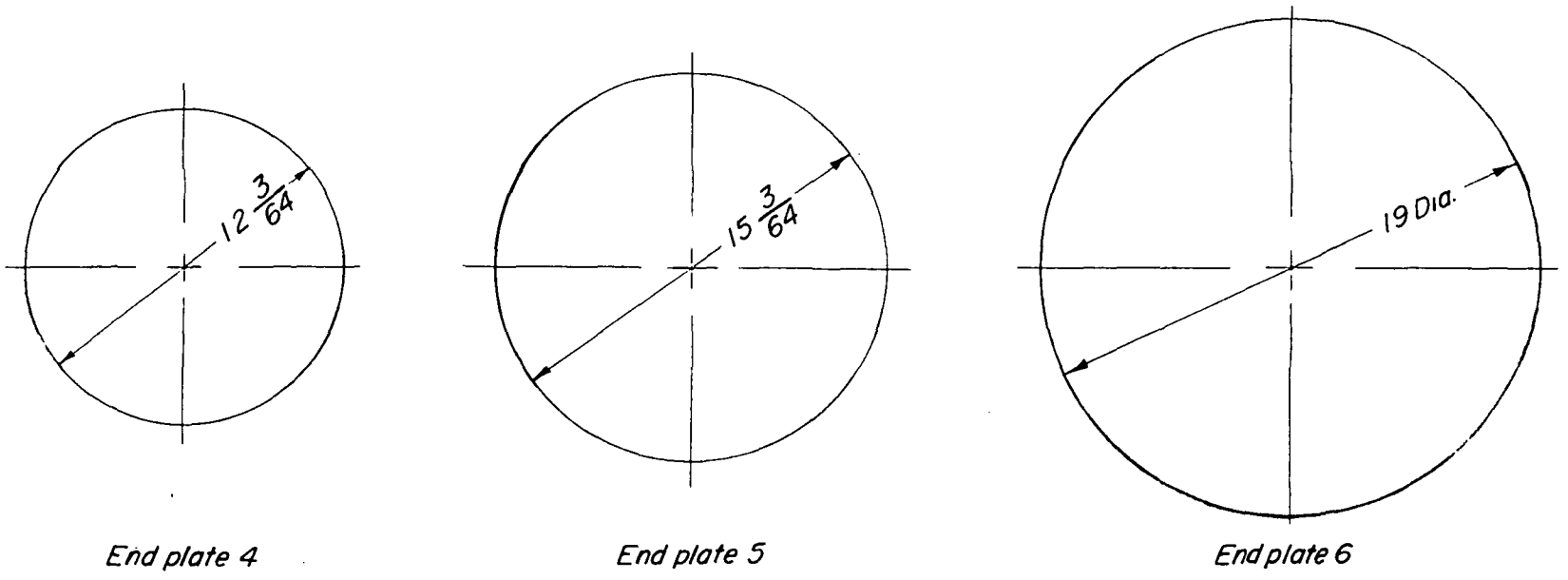

(b) End plates 4, 5, and 6.

Figure 4.- Continued.

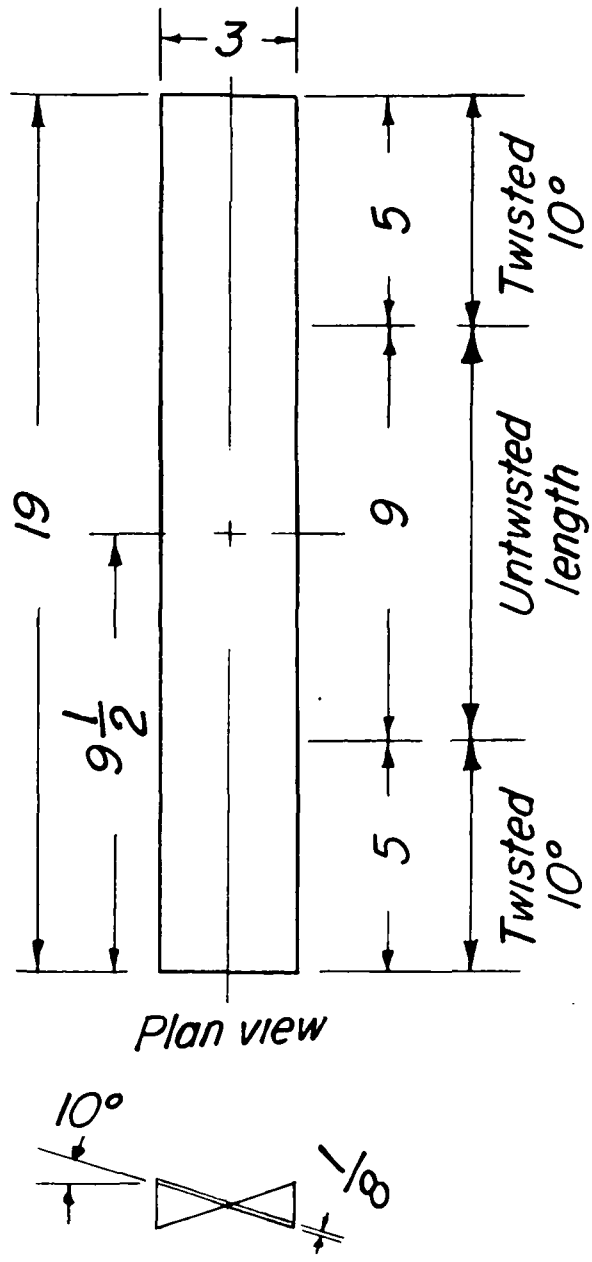

End plate 7

(c) End plate 7.

Figure 4.- Concluded.

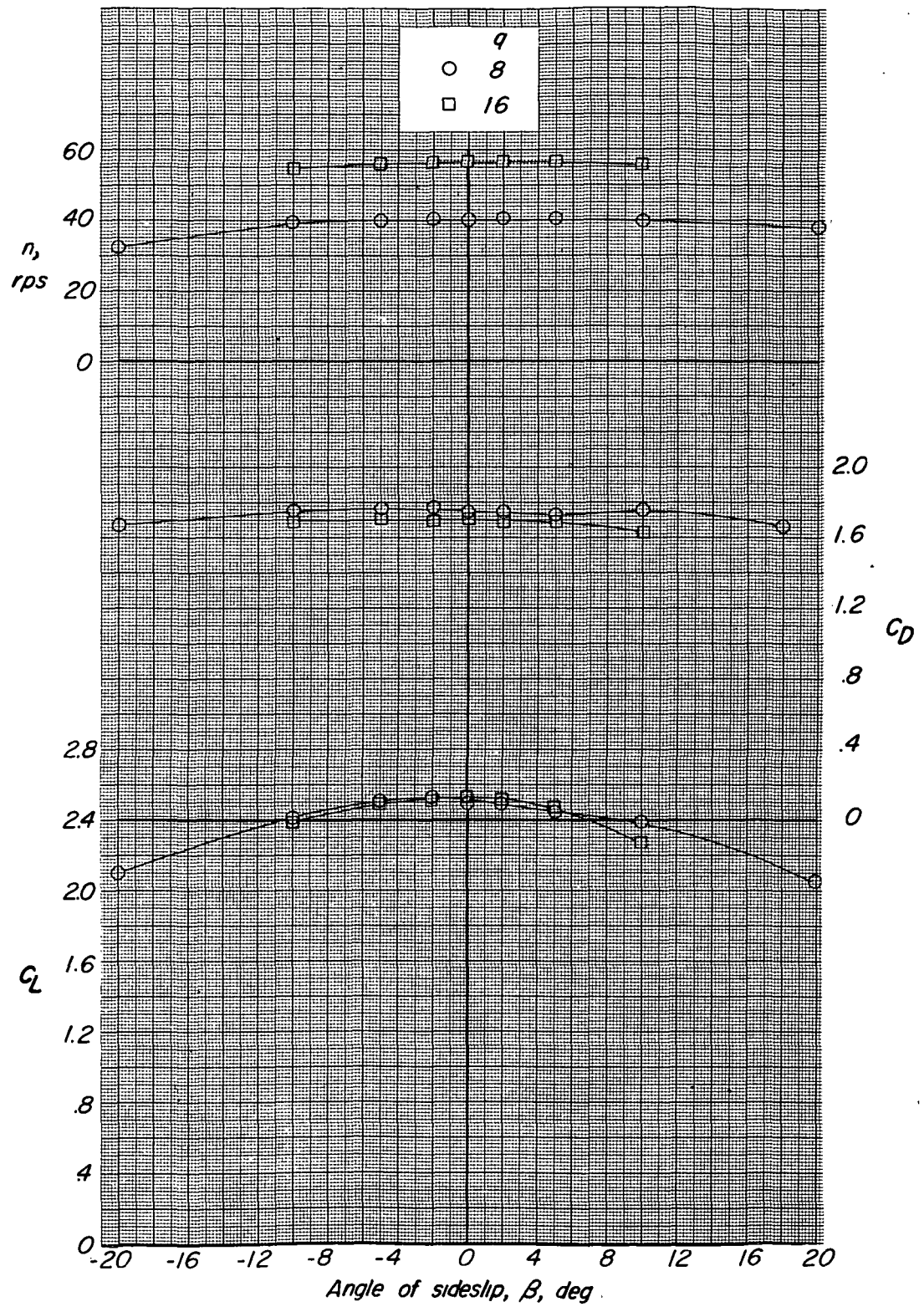

Figure 5.- Variation of C_L, C_D, and n with angle of sideslip β. Model 1; q = 8 and 16.

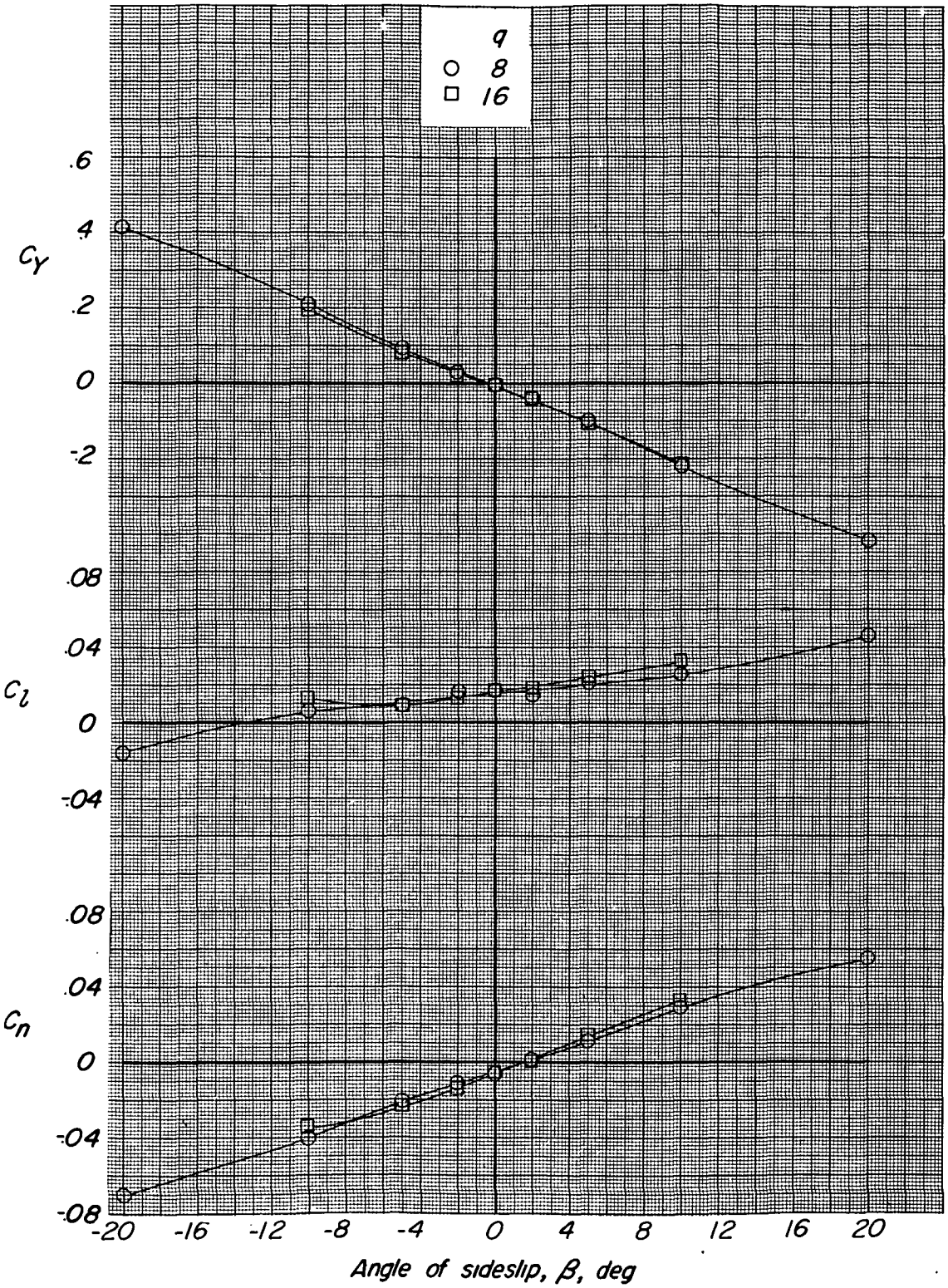

Figure 6.- Variation of C_n, C_l, and C_Y with angle of sideslip β. Model 1; q = 8 and 16.

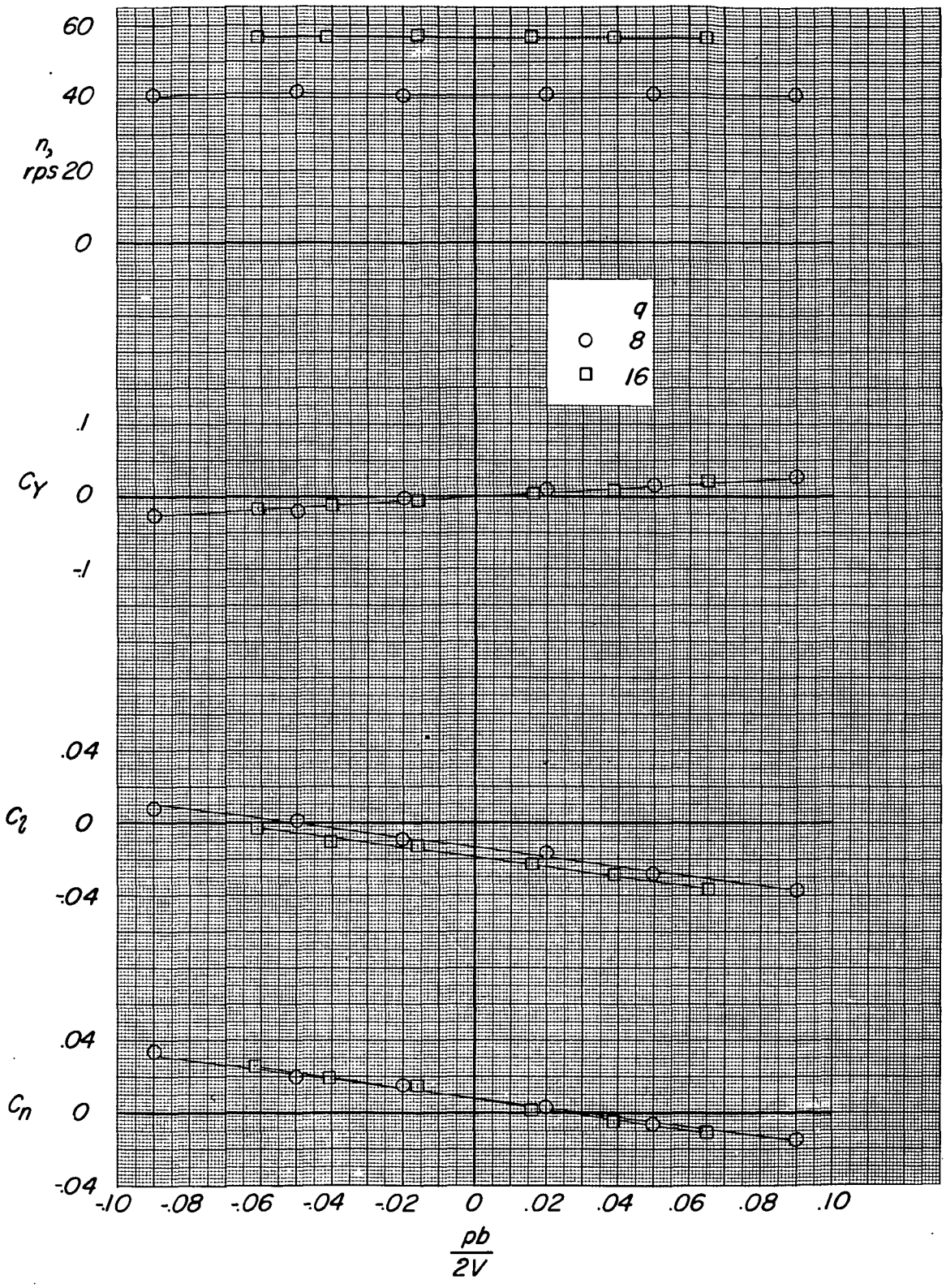

Figure 7.- Variation of C_n, C_l, C_Y, and n with pb/2V for $\beta = 0$. Model 1; q = 8 and 16.

Figure 8.- Variation of C_{n_p}, C_{l_p}, and C_{Y_p} with angle of sideslip β. Model 1; q = 8 and 16.

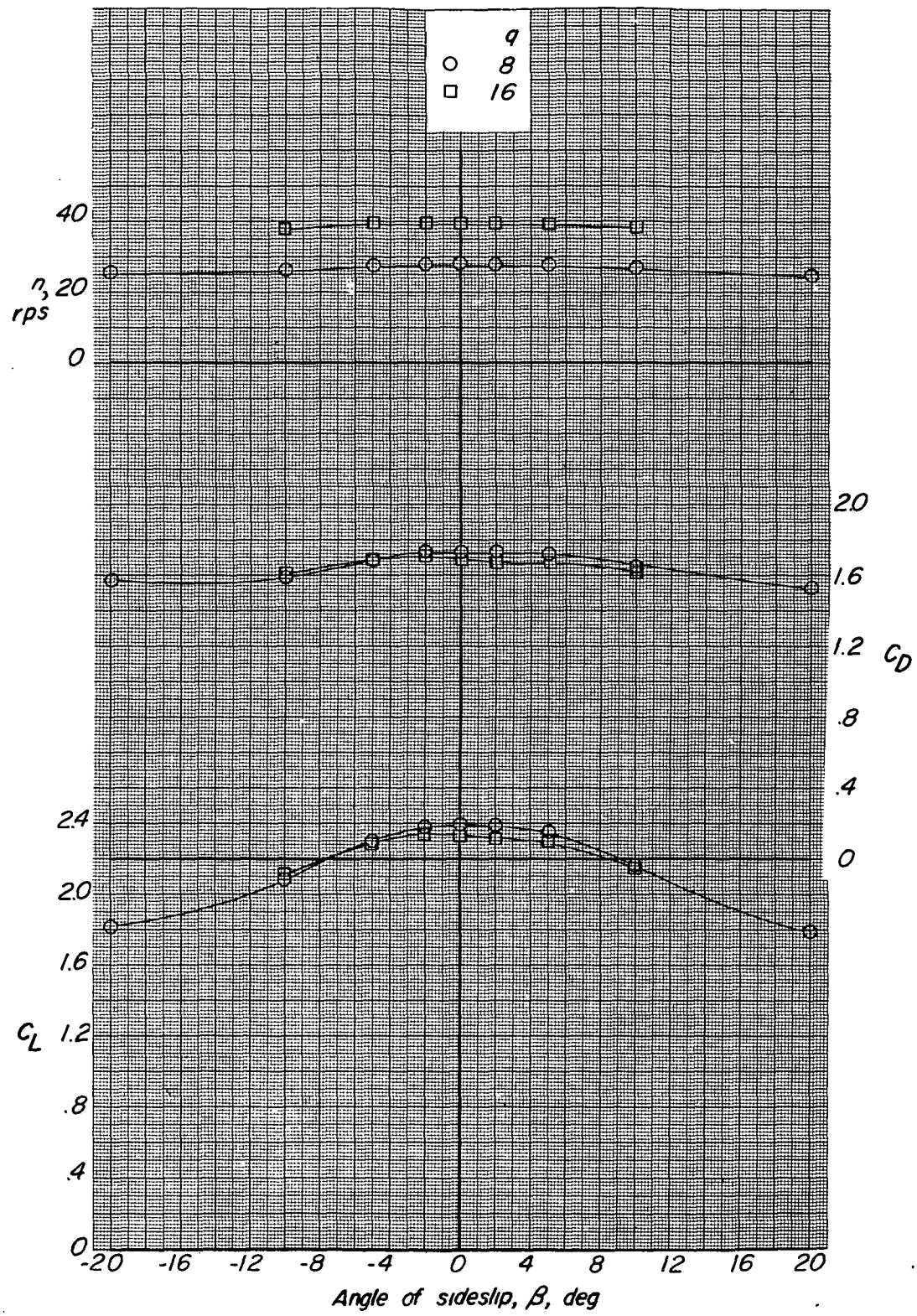

Figure 9.- Variation of C_L, C_D, and n with angle of sideslip β. Model 2; q = 8 and 16.

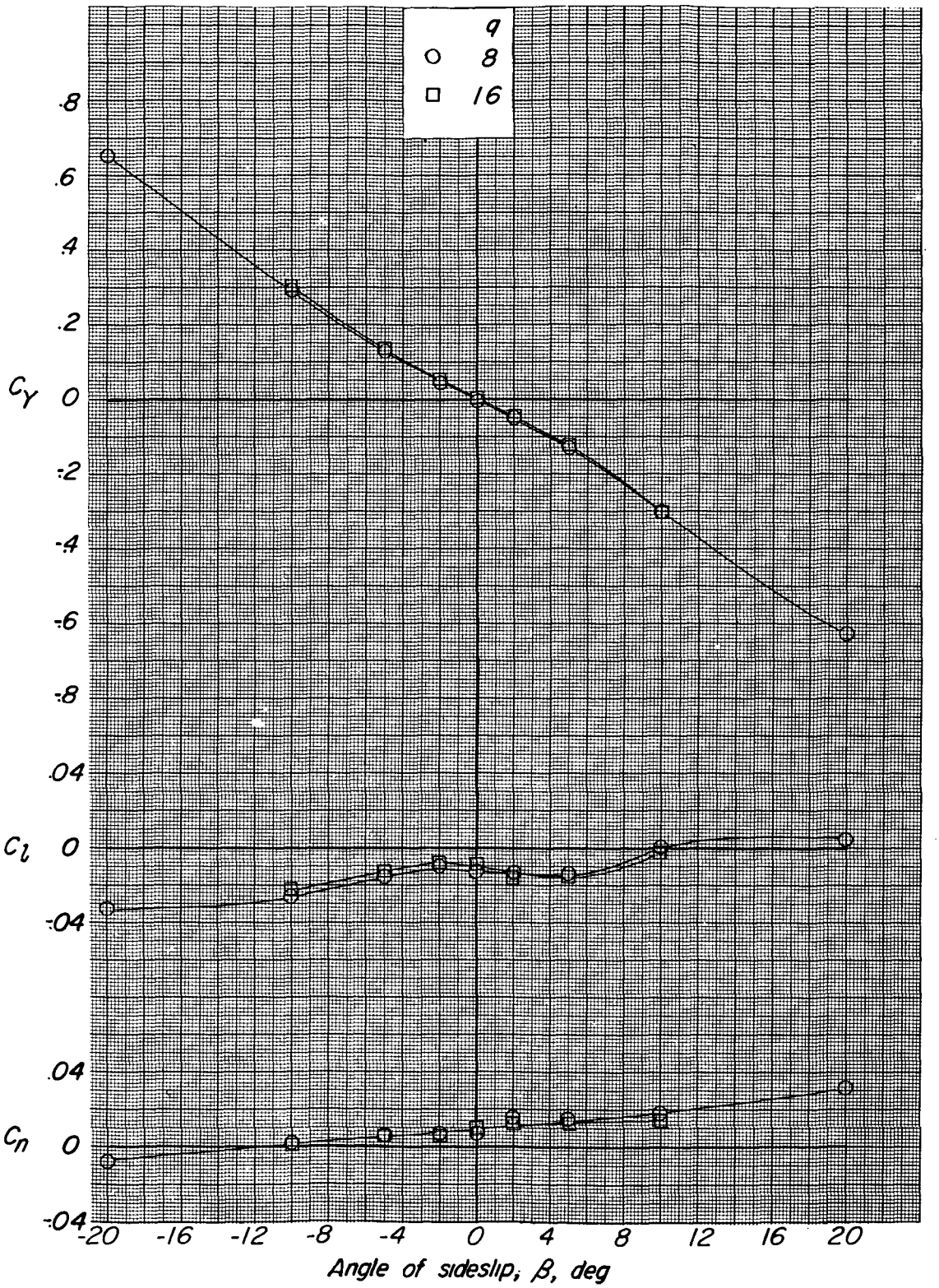

Figure 10.- Variation of C_n, C_l, and C_Y with angle of sideslip β. Model 2; q = 8 and 16.

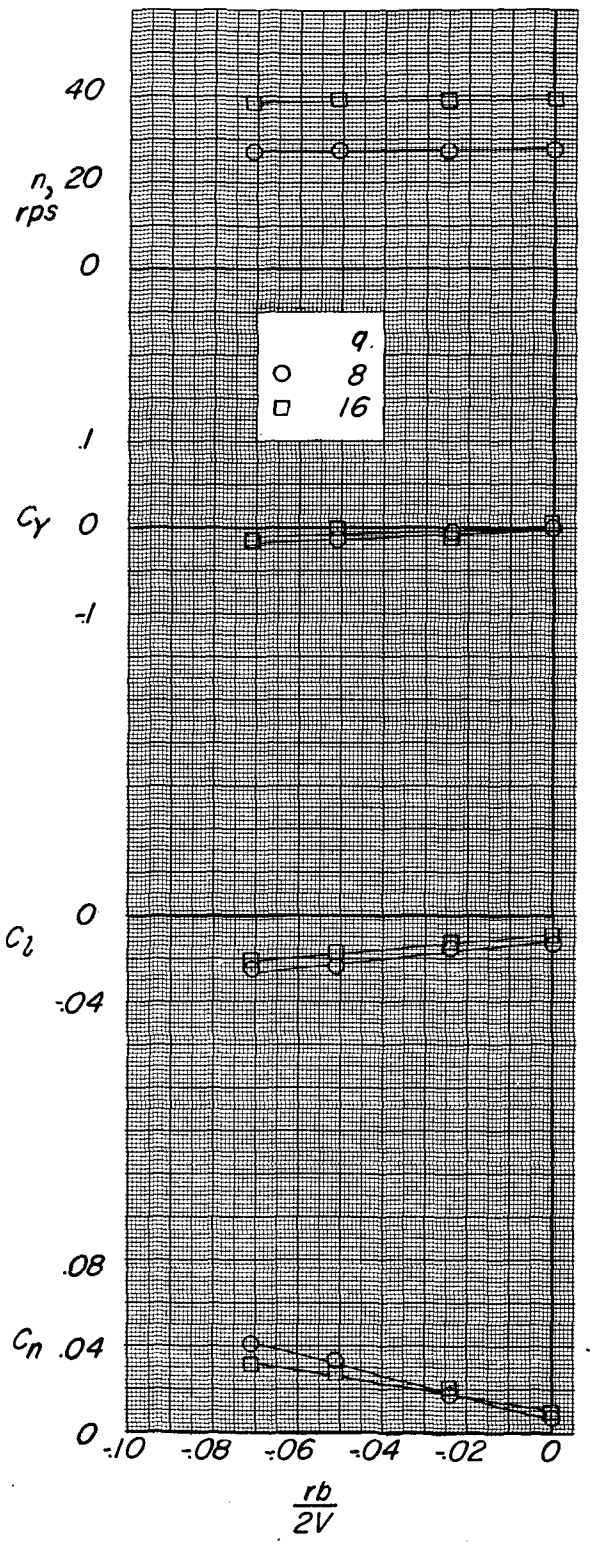

Figure 11.- Variation of C_n, C_l, C_Y, and n with rb/2V for $\beta = 0$. Model 2; q = 8 and 16.

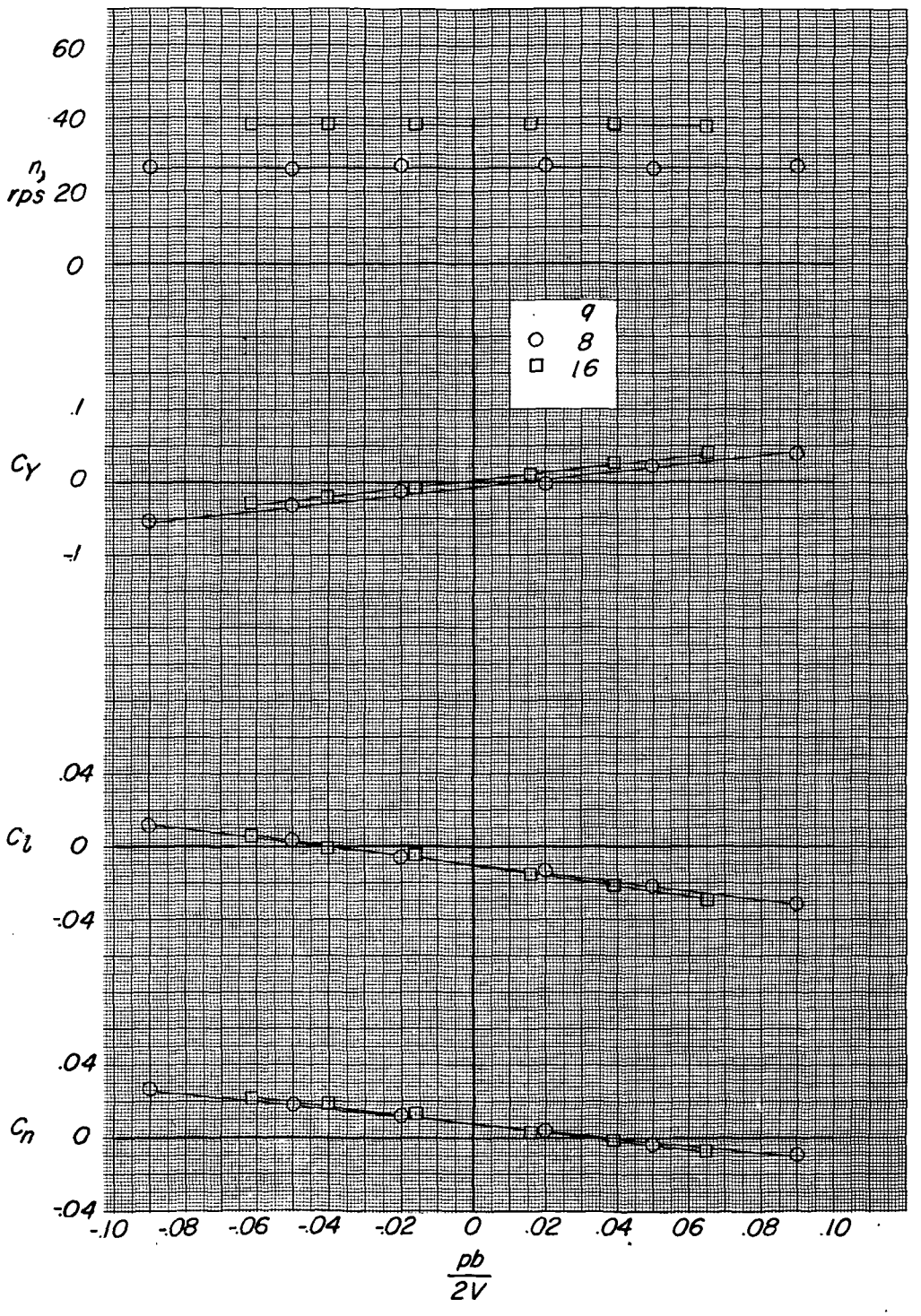

Figure 12.- Variation of C_n, C_l, C_Y, and n with pb/2V for $\beta = 0$. Model 2; q = 8 and 16.

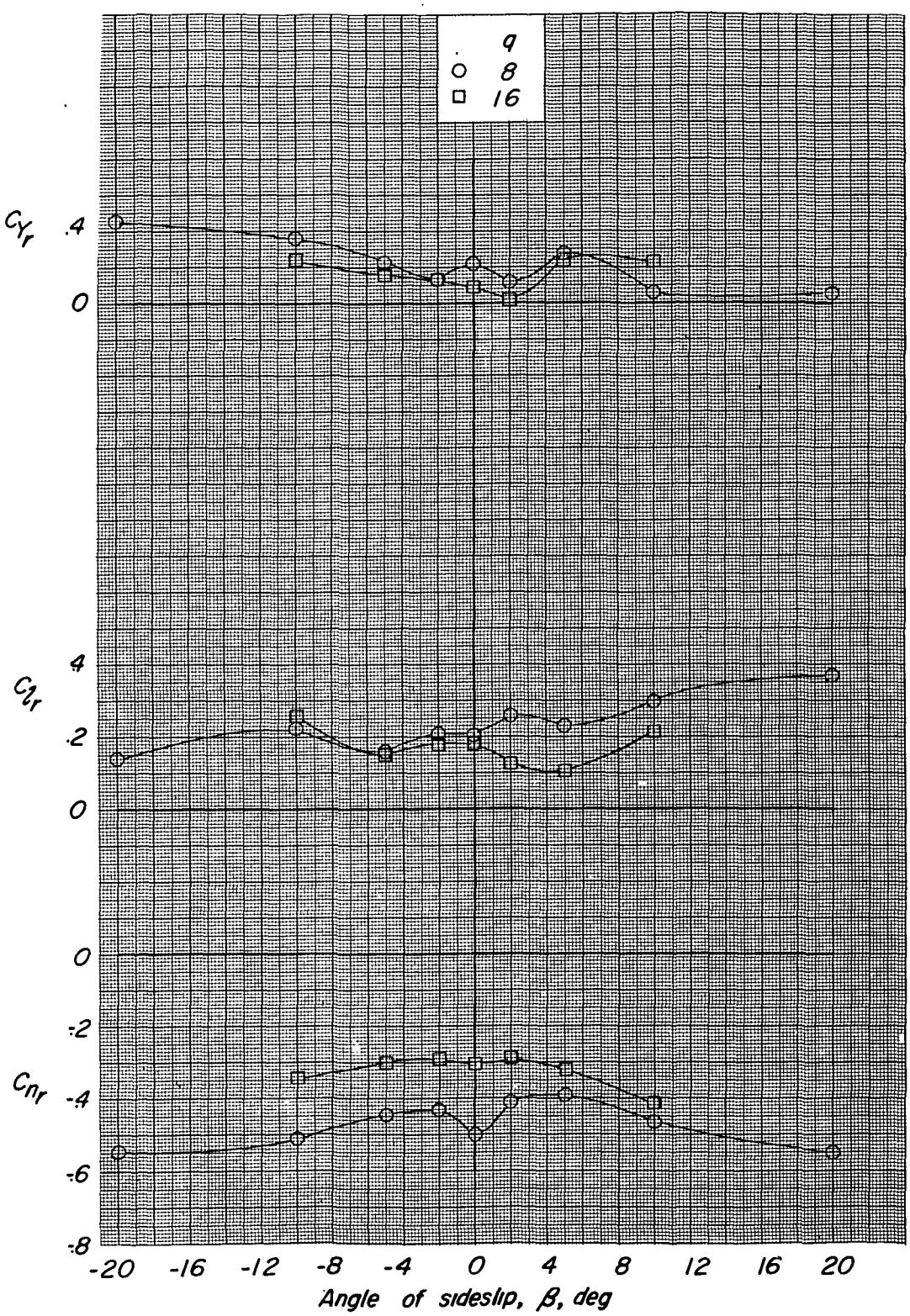

Figure 13.- Variation of C_{n_r}, C_{l_r}, and C_{Y_r} with angle of sideslip β. Model 2; q = 8 and 16.

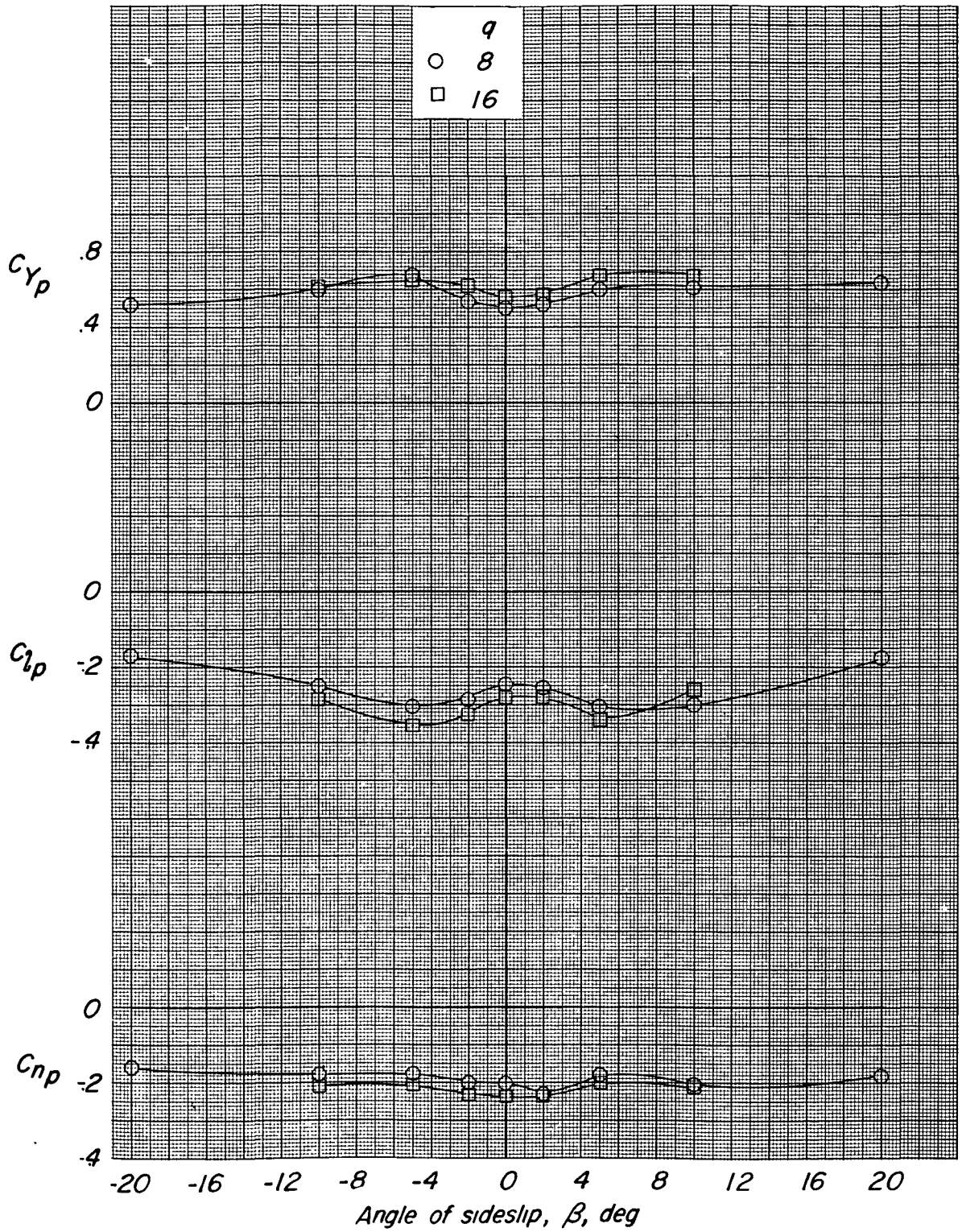

Figure 14.- Variation of C_{n_p}, C_{l_p}, and C_{Y_p} with angle of sideslip β. Model 2; q = 8 and 16.

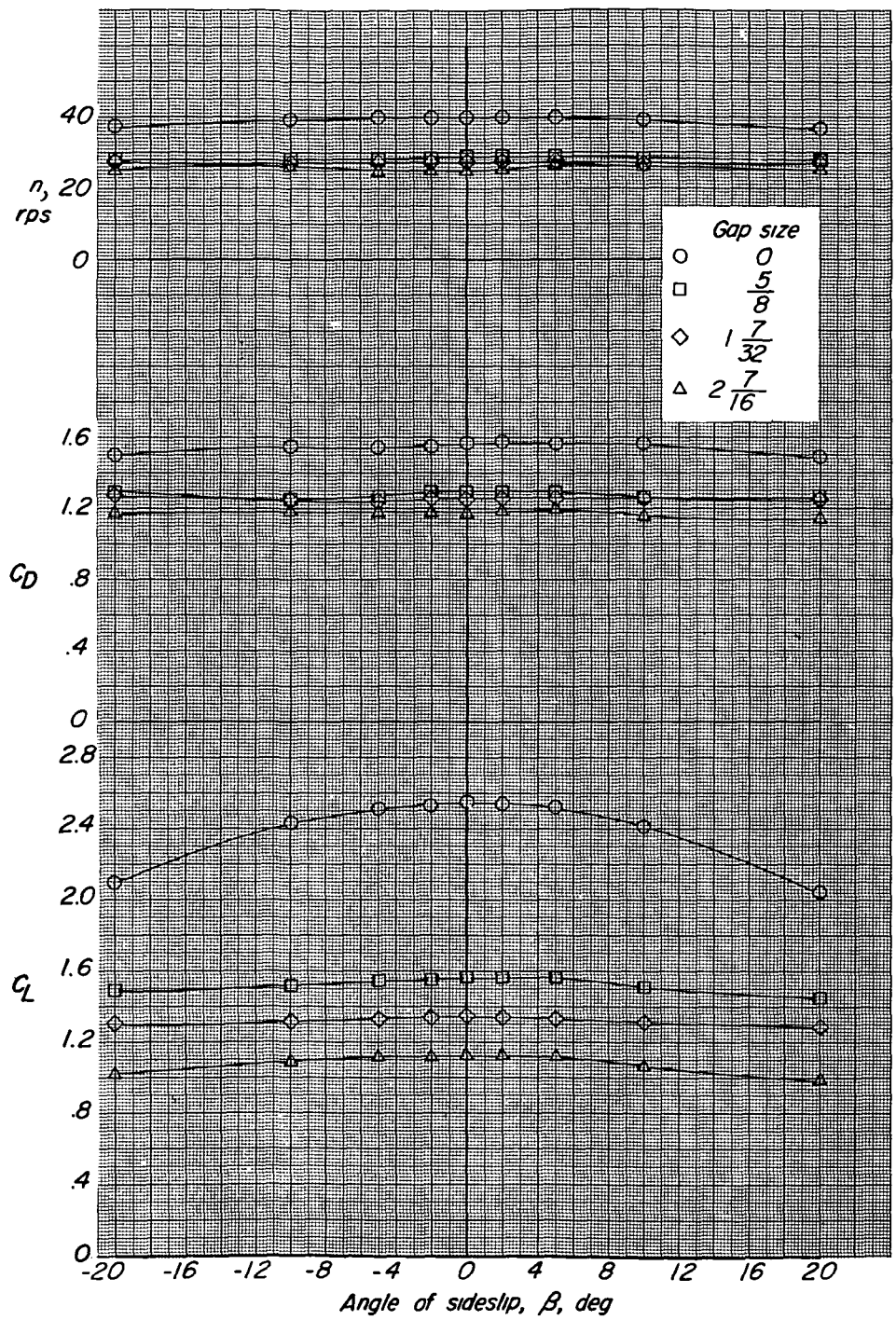

Figure 15.- Variation of C_L, C_D, and n with angle of sideslip β for model 3 with different size gaps. End plate 1; driving vane on; q = 8.

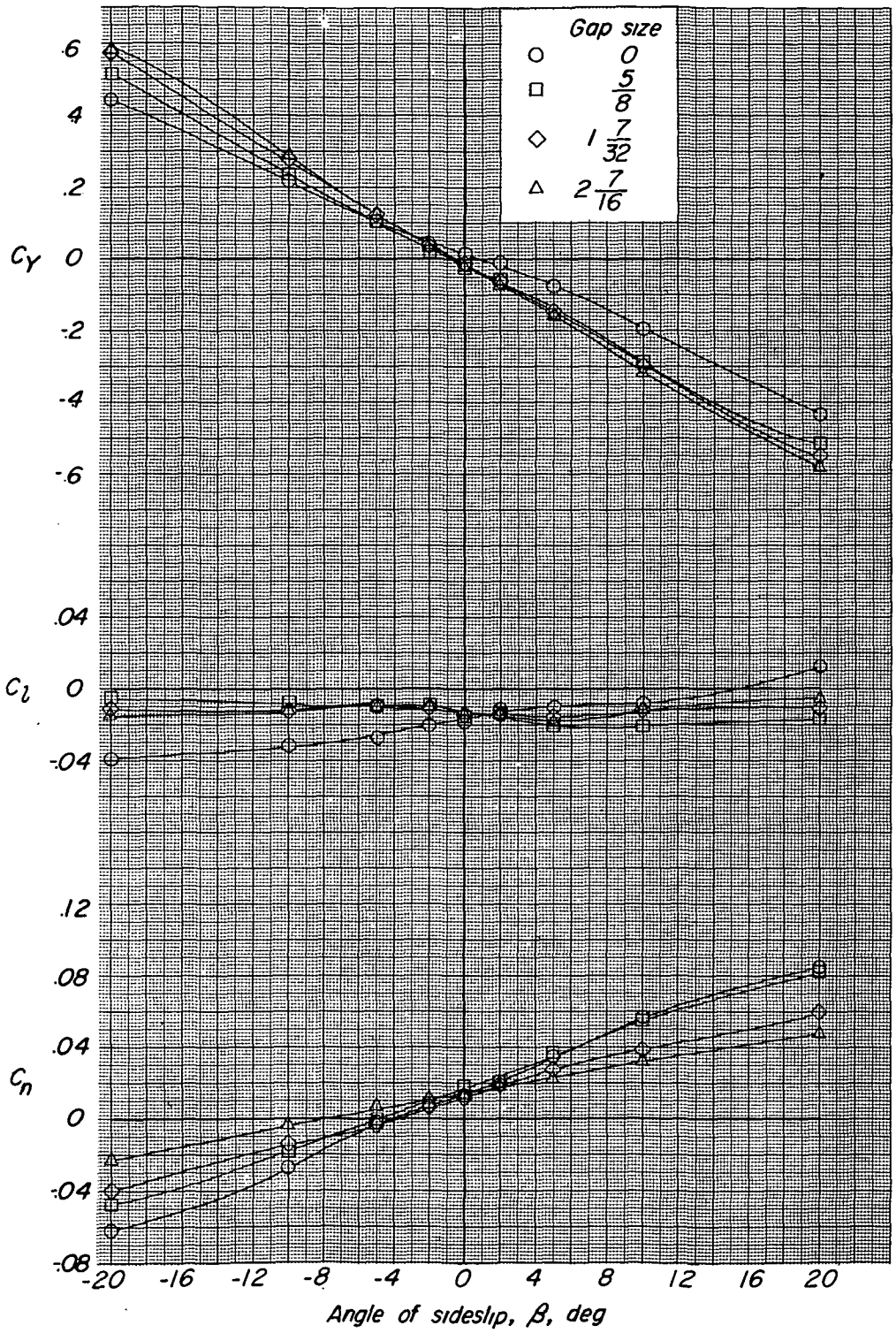

Figure 16.- Variation of C_n, C_l, and C_Y with angle of sideslip β for model 3 with different size gaps. End plate 1; driving vane on; $q = 8$.

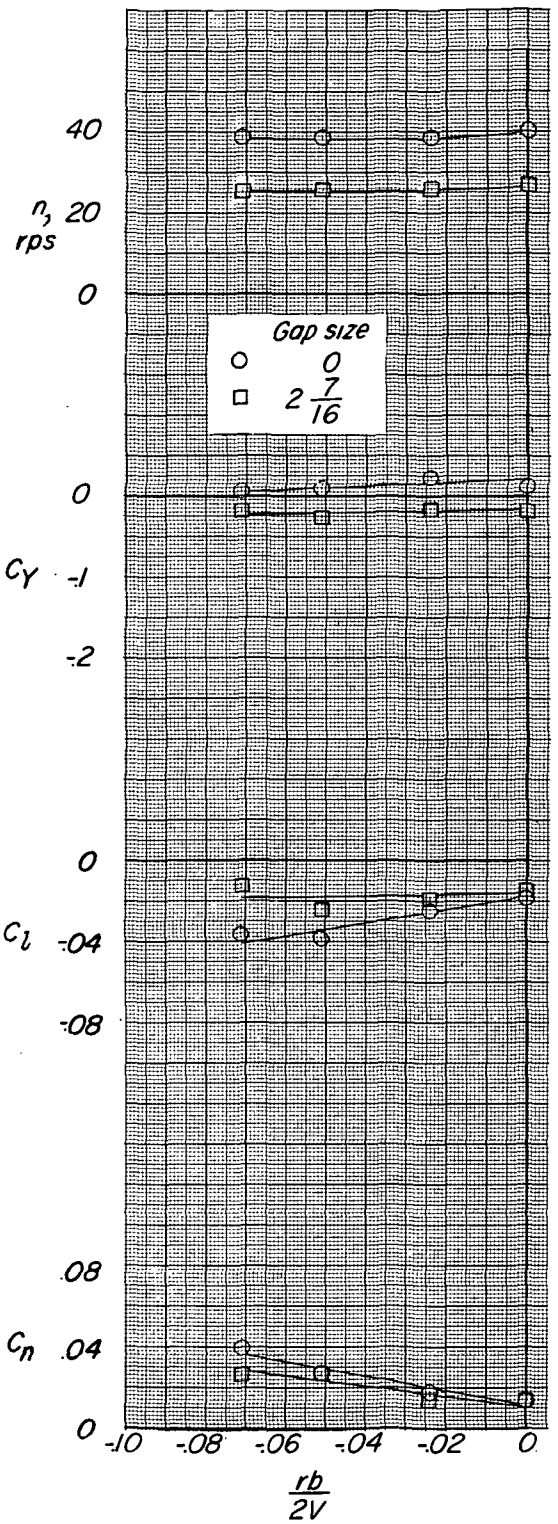

Figure 17.- Variation of C_n, C_l, C_Y, and n with rb/2V for model 3 with 0- and $2\frac{7}{16}$-inch gap size. End plate 1; driving vane on; q = 8.

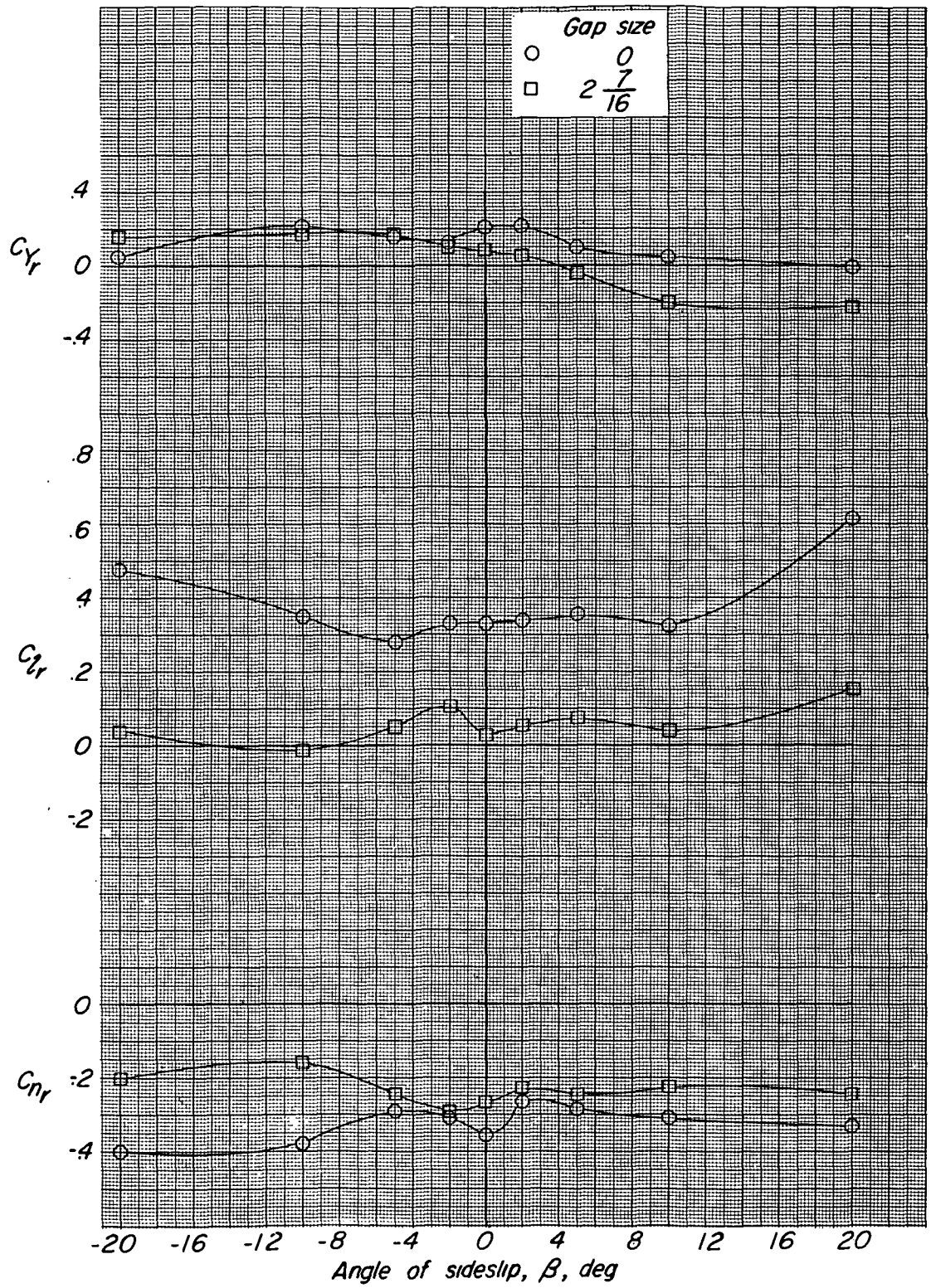

Figure 18.- Variation of C_{n_r}, C_{l_r}, and C_{Y_r} with angle of sideslip β for model 3 with 0- and $2\frac{7}{16}$-inch gap size. End plate 1; driving vane on; $q = 8$.

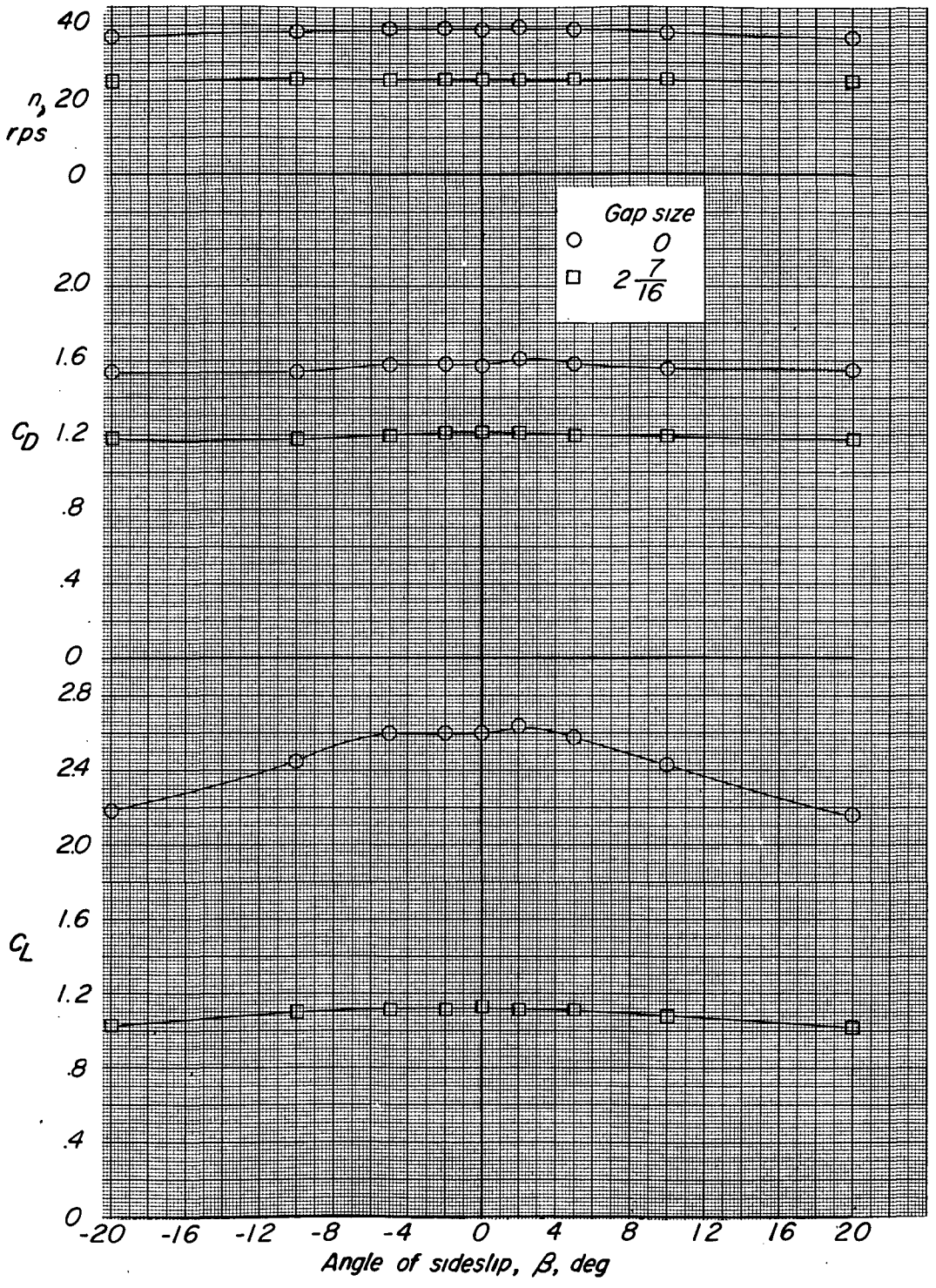

Figure 19.- Variation of C_L, C_D, and n with angle of sideslip β for model 3 with 0- and $2\frac{7}{16}$-inch gap size. End plate 2; driving vane on; q = 8.

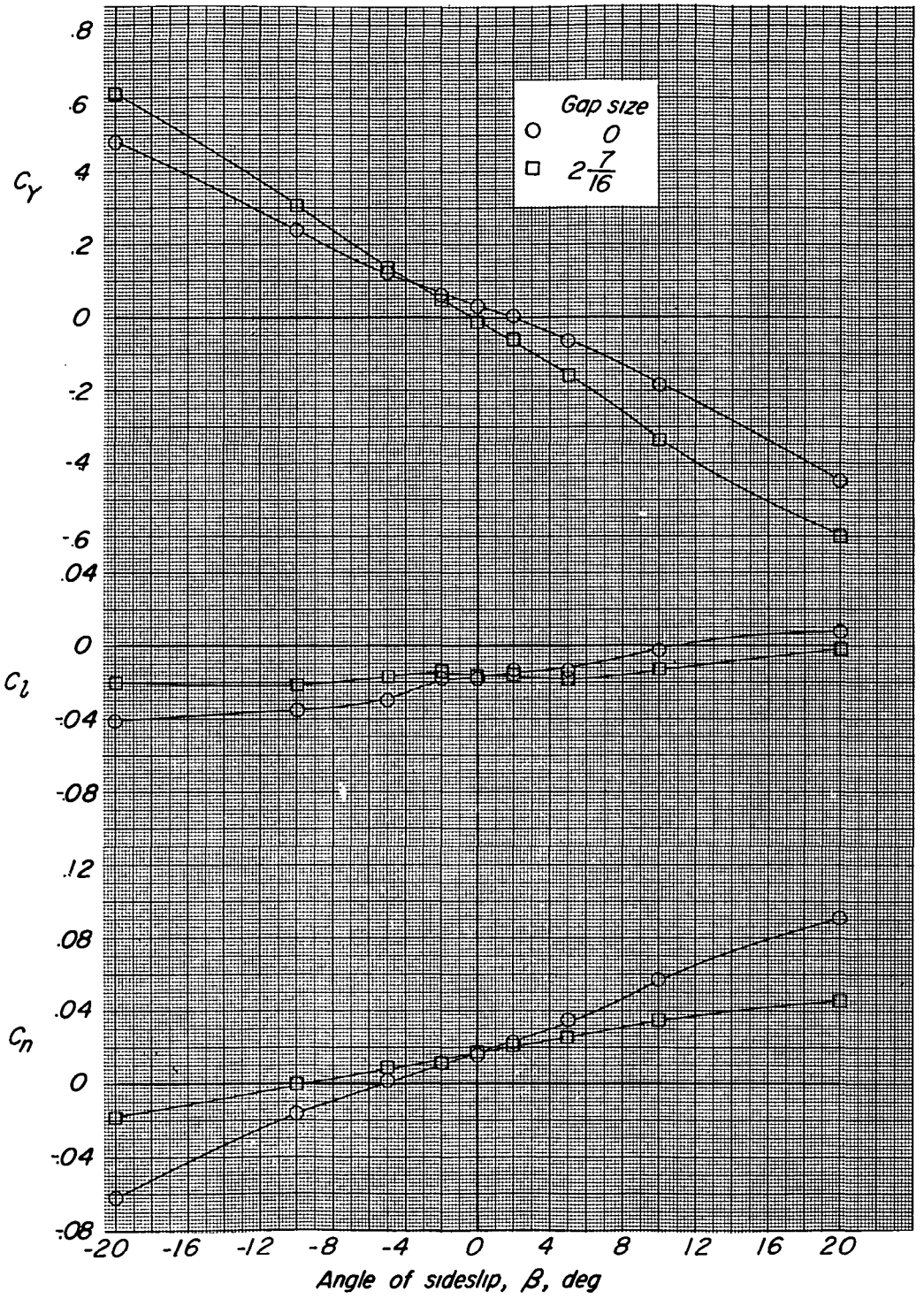

Figure 20.- Variation of C_n, C_l, and C_Y with angle of sideslip β for model 3 with 0- and $2\frac{7}{16}$-inch gap size. End plate 2; driving vane on; q = 8.

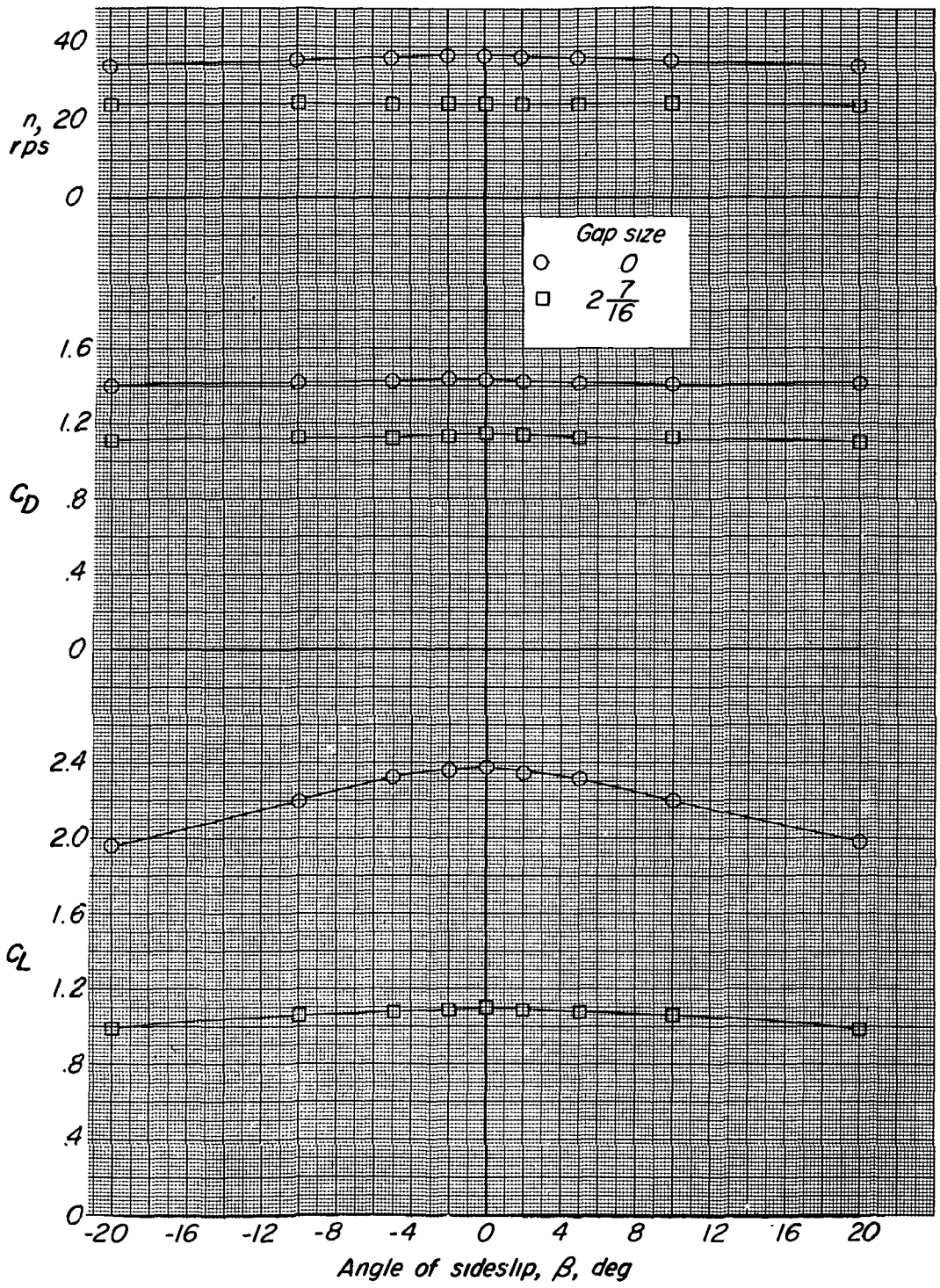

Figure 21.- Variation of C_L, C_D, and n with angle of sideslip β for model 3 with 0- and $2\frac{7}{16}$-inch gap size. End plate 3 with long dimension perpendicular to chord; driving vane on; q = 8.

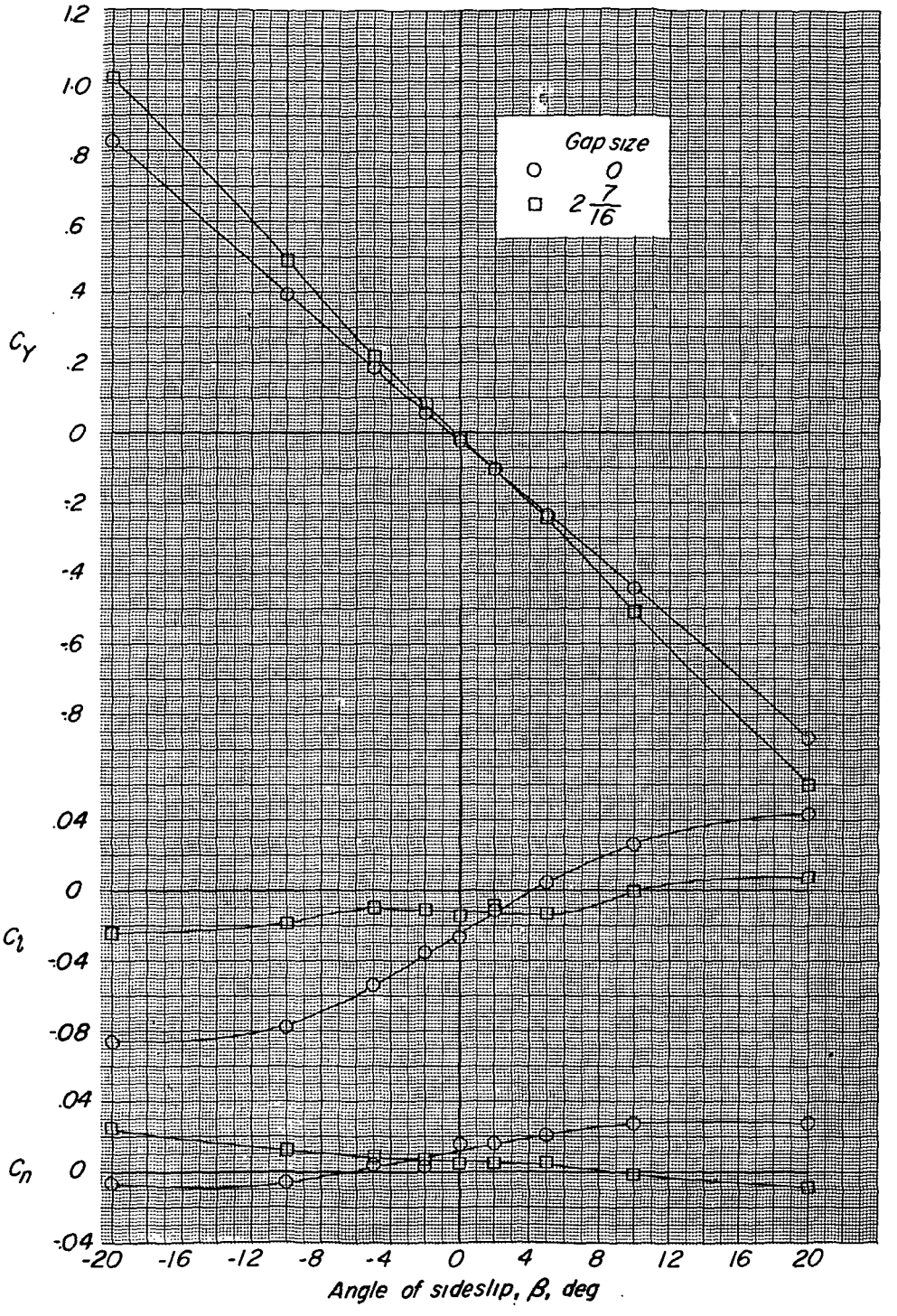

Figure 22.- Variation of C_n, C_l, and C_Y with angle of sideslip β for model 3 with 0- and $2\frac{7}{16}$-inch gap size. End plate 3 with long dimension perpendicular to chord; driving vane on; q = 8.

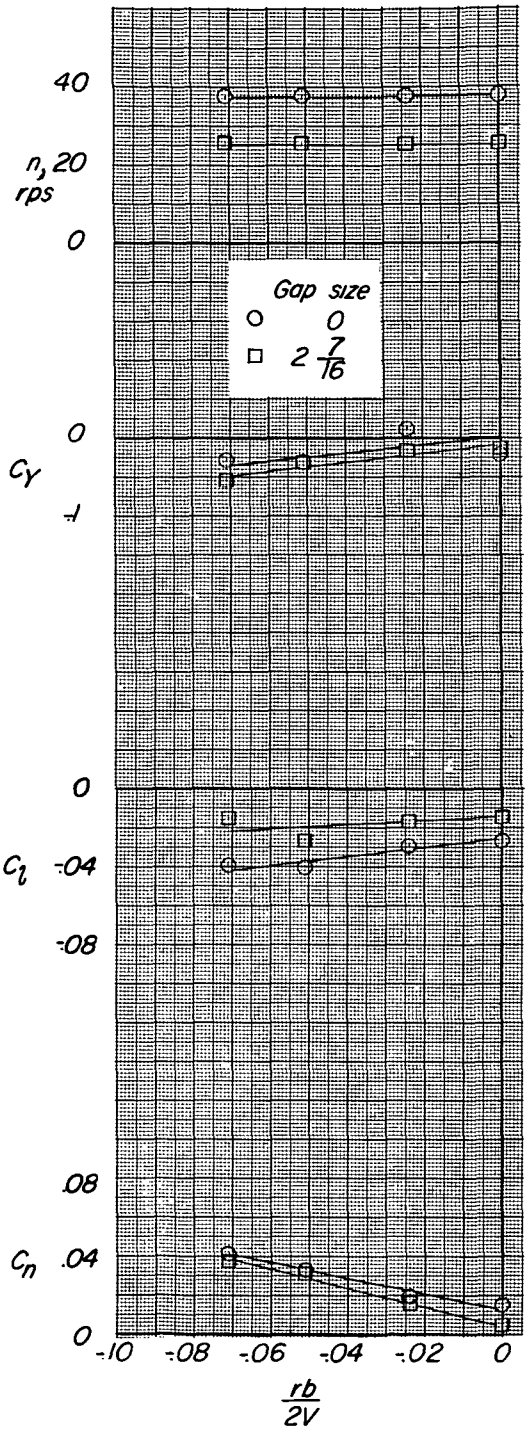

Figure 23.- Variation of C_n, C_l, C_Y, and n with rb/2V for model 3 with 0- and $2\frac{7}{16}$-inch gap size. End plate 3 with long dimension perpendicular to chord; driving vane on; q = 8.

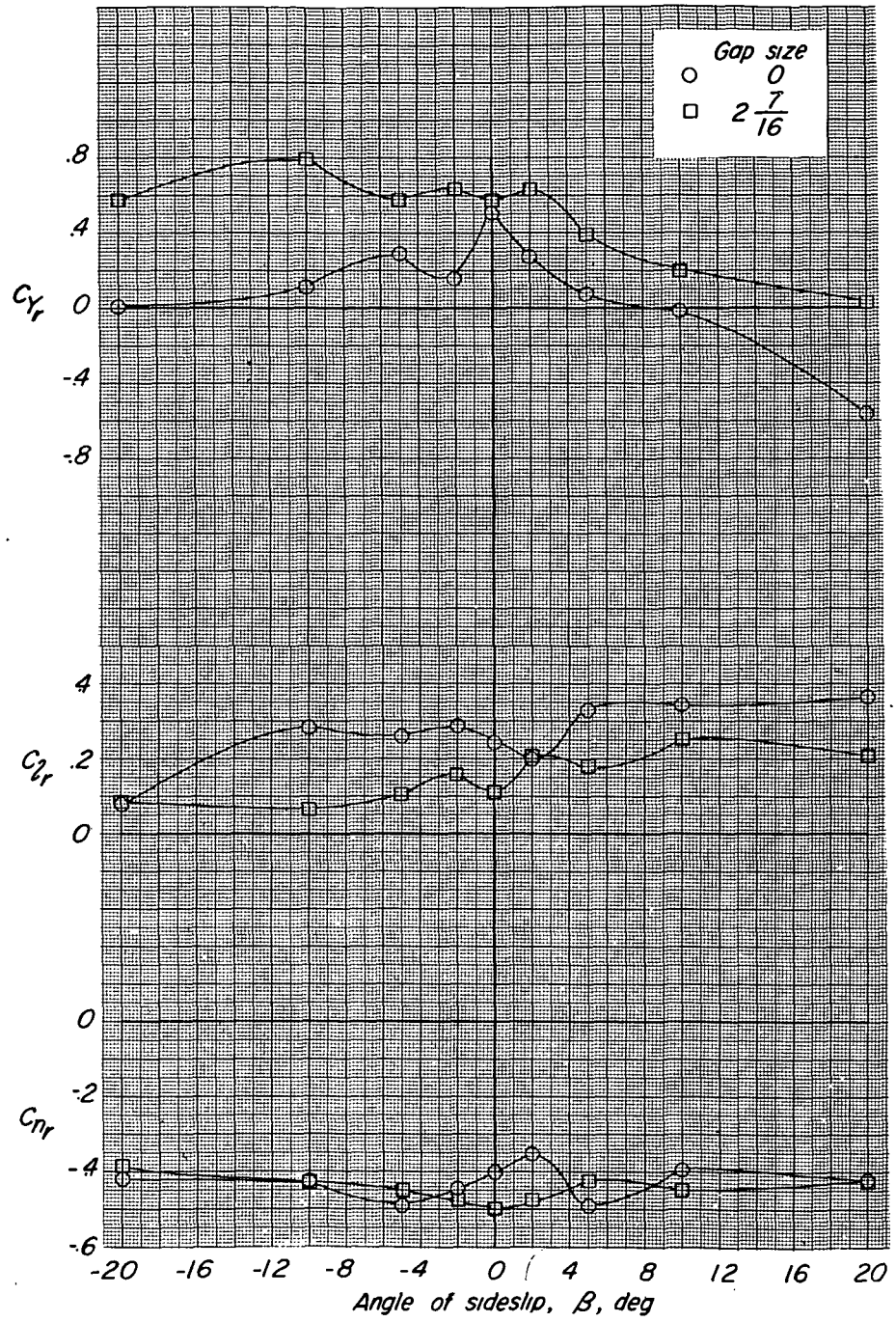

Figure 24.- Variation of C_{n_r}, C_{l_r}, and C_{Y_r} with angle of sideslip β for model 3 with 0- and $2\frac{7}{16}$-inch gap size. End plate 3 with long dimension perpendicular to chord; driving vane on; $q = 8$.

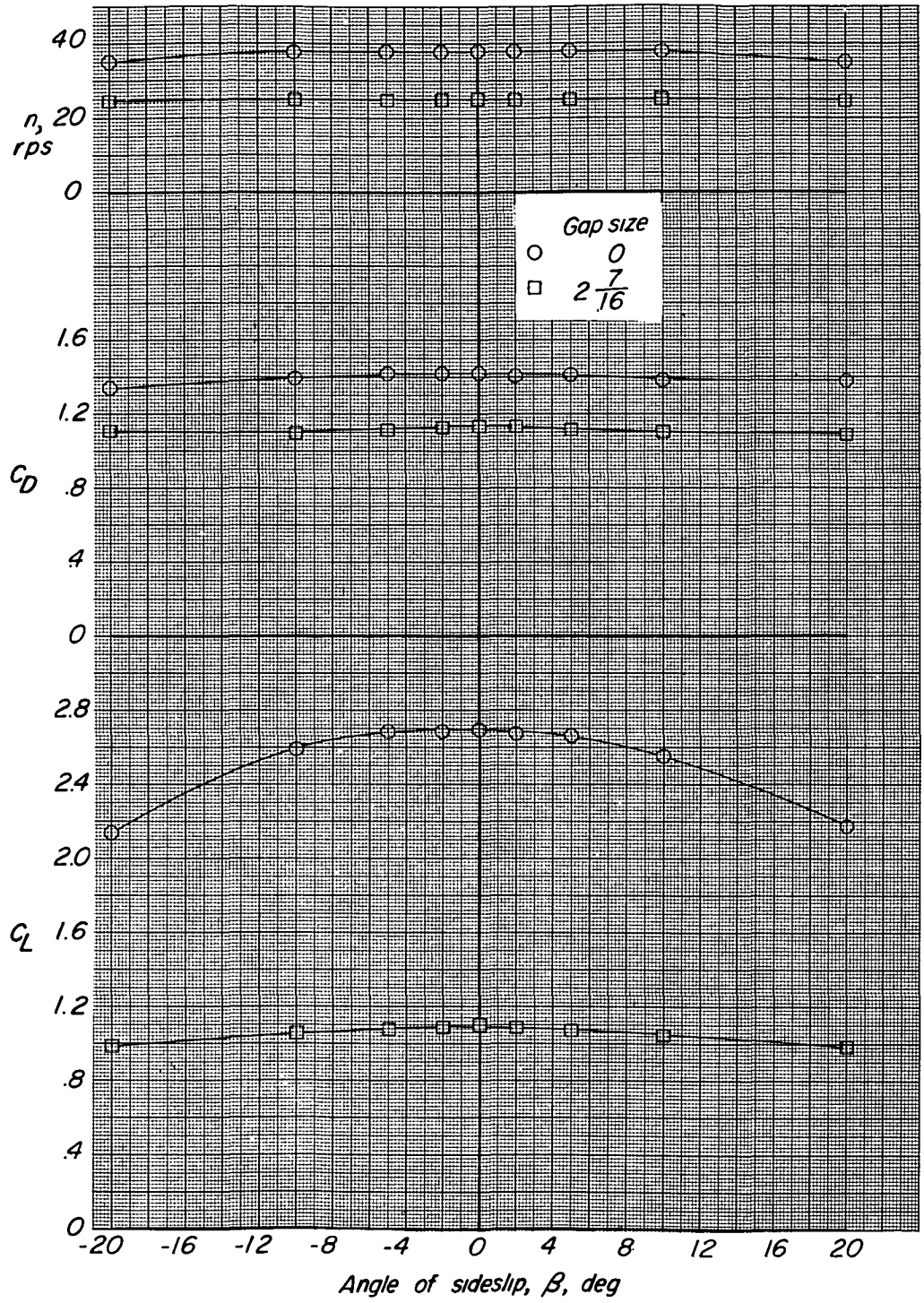

Figure 25.- Variation of C_L, C_D, and n with angle of sideslip β for model 3 with 0- and $2\frac{7}{16}$ - inch gap size. End plate 3 with long dimension parallel to chord; driving vane on; q = 8.

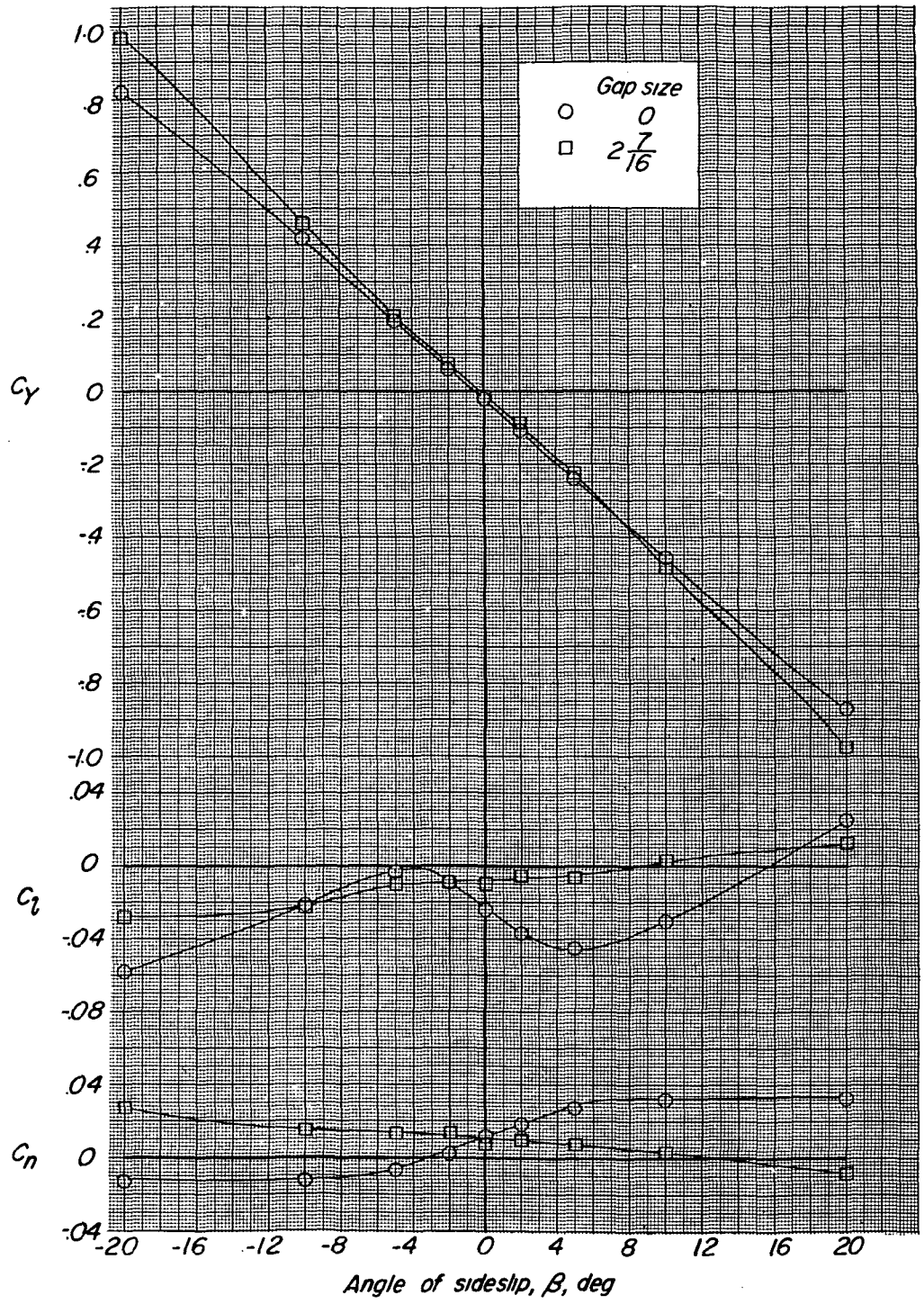

Figure 26.- Variation of C_n, C_l, and C_Y with angle of sideslip β for model 3 with 0- and $2\frac{7}{16}$-inch gap size. End plate 3 with long dimension parallel to chord; driving vane on; $q = 8$.

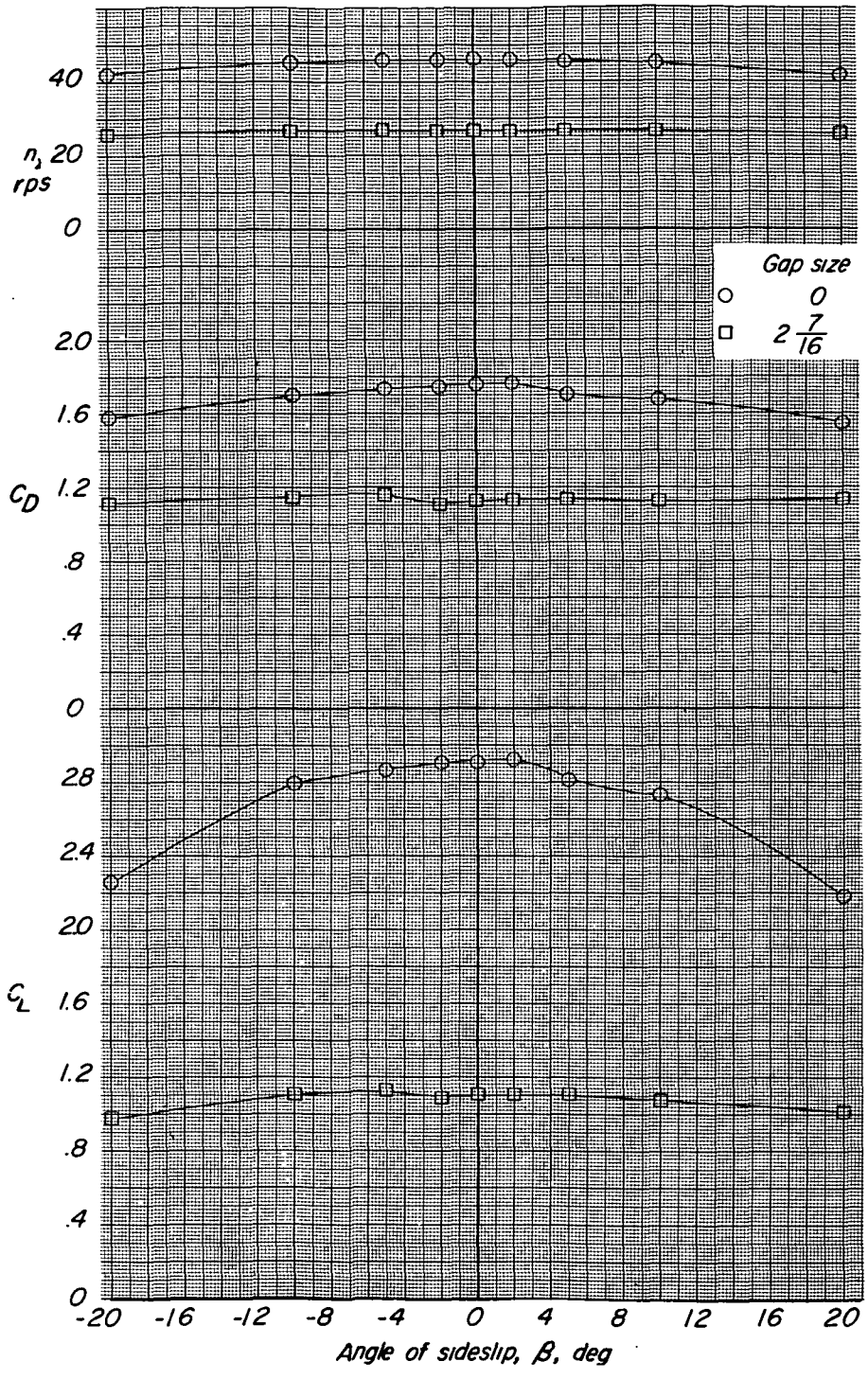

Figure 27.- Variation of C_L, C_D, and n with angle of sideslip β for model 3 with 0- and $2\frac{7}{16}$-inch gap size. End plate 4; driving vane on; q = 8.

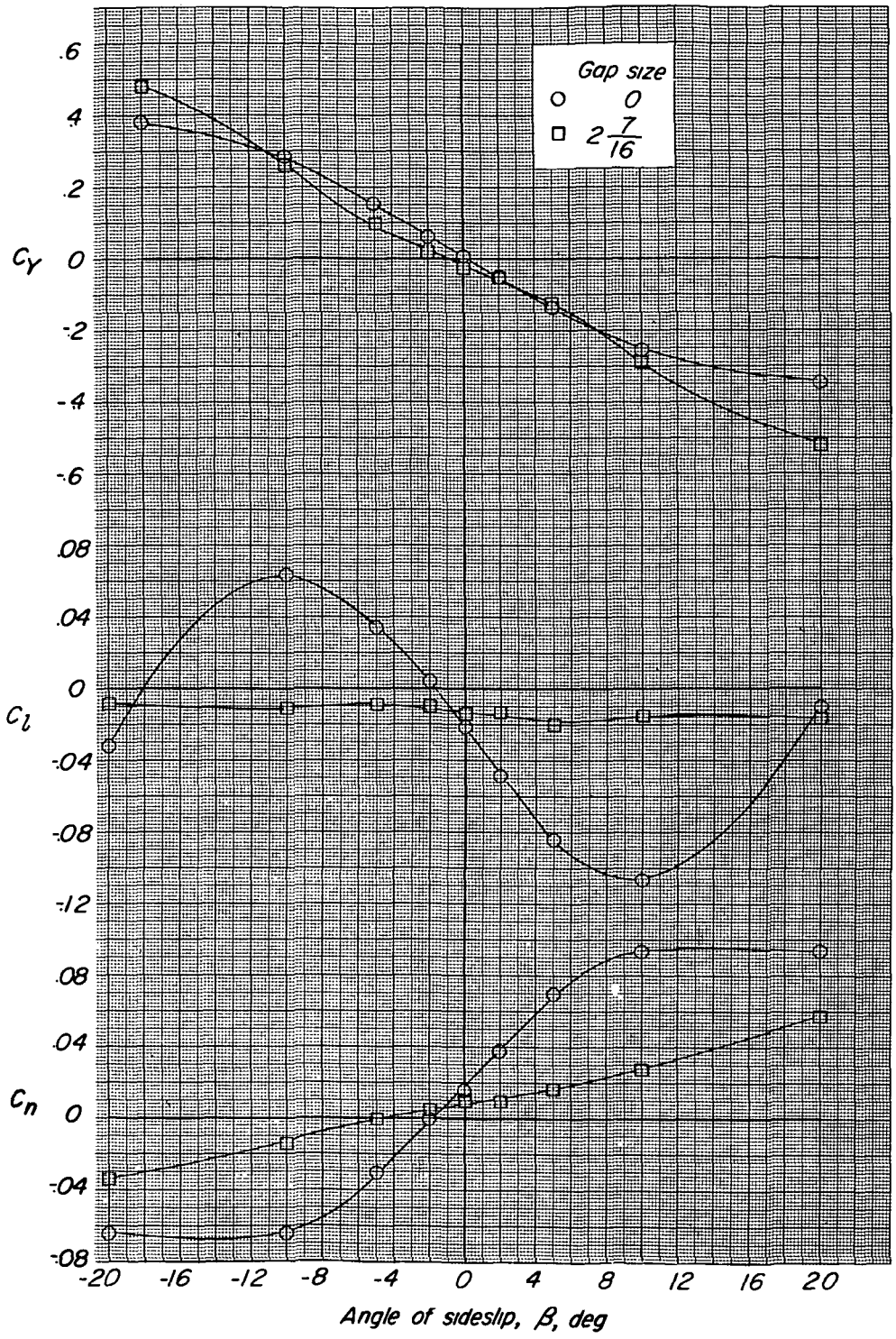

Figure 28.- Variation of C_n, C_l, and C_r with angle of sideslip β for model 3 with 0- and $2\frac{7}{16}$-inch gap size. End plate 4; driving vane on; $q = 8$.

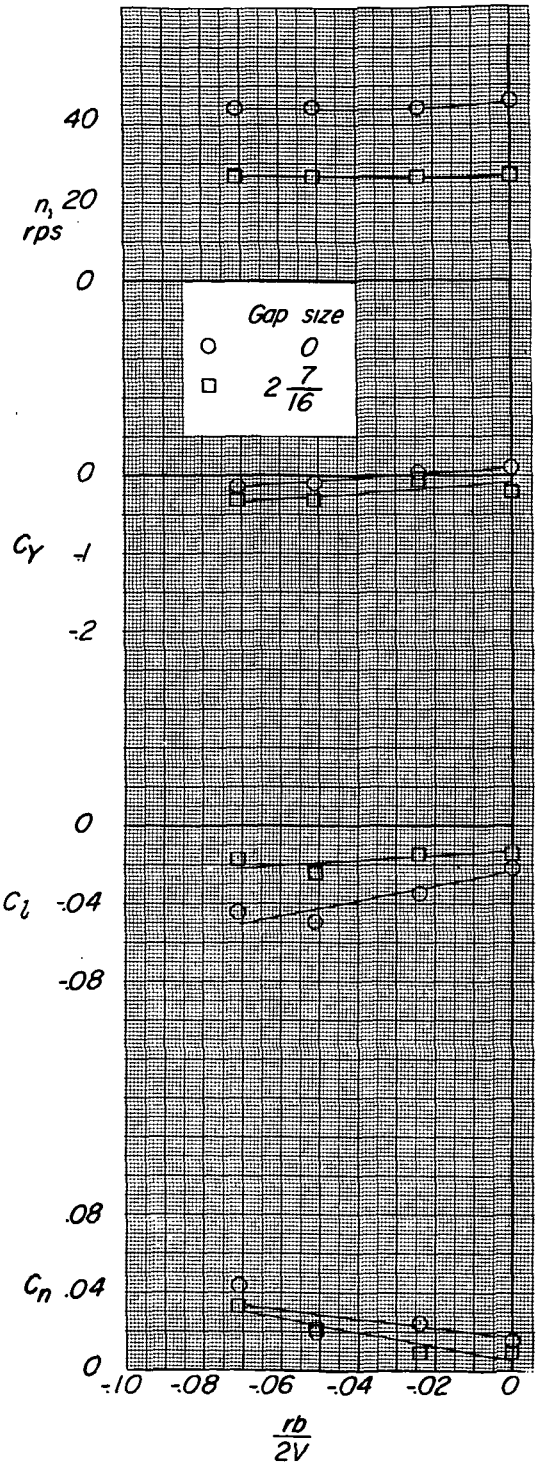

Figure 29.- Variation of C_n, C_l, C_Y, and n with rb/2V for model 3 with 0- and $2\frac{7}{16}$ - inch gap size. End plate 4; driving vane on; q = 8.

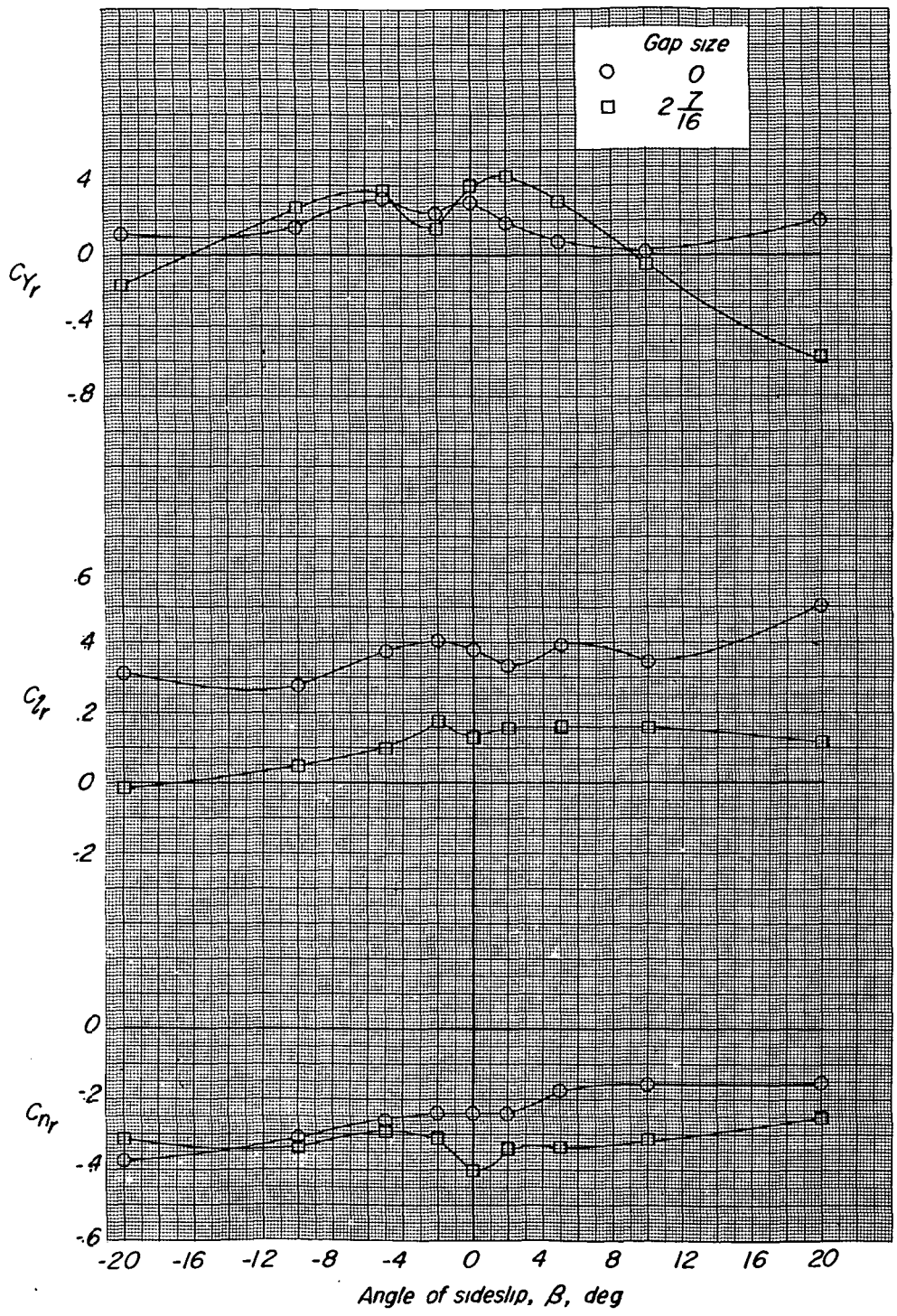

Figure 30.- Variation of C_{n_r}, C_{l_r}, and C_{Y_r} with angle of sideslip β for model 3 with 0- and $2\frac{7}{16}$- inch gap size. End plate 4; driving vane on; $q = 8$.

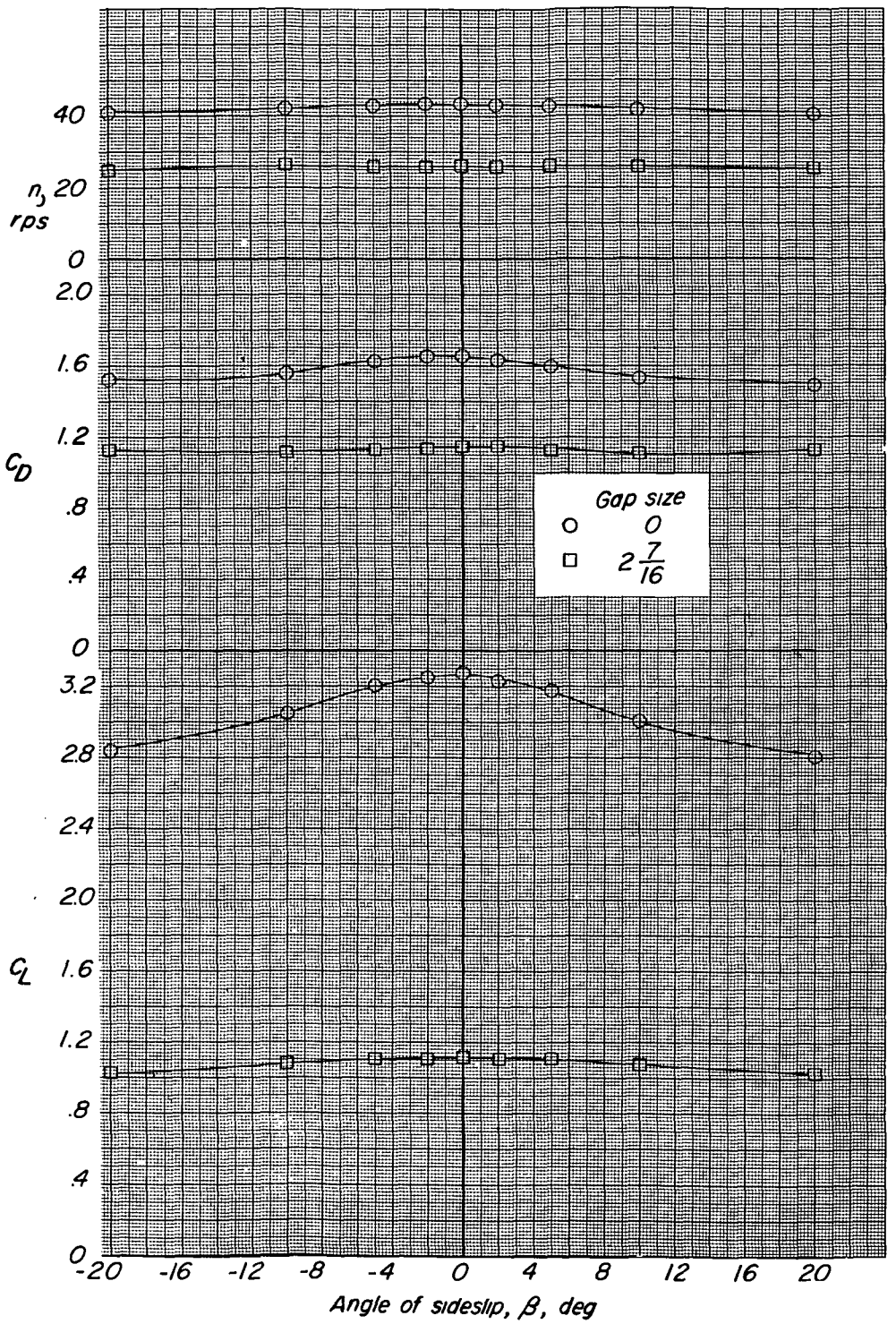

Figure 31.- Variation of C_L, C_D, and n with angle of sideslip β for model 3 with 0- and $2\frac{7}{16}$- inch gap size. End plate 5; driving vane on; q = 8.

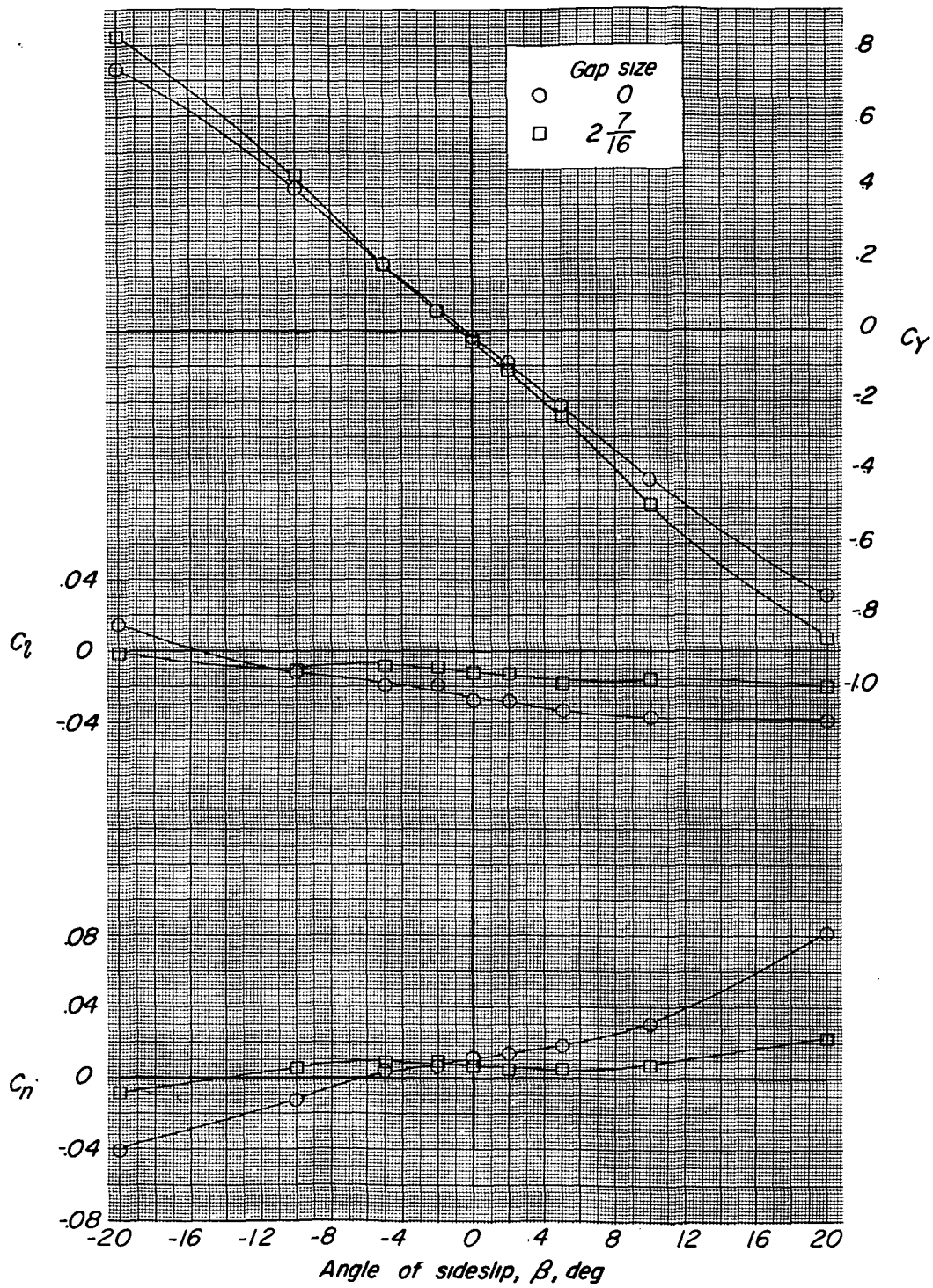

Figure 32.- Variation of C_n, C_l, and C_Y with angle of sideslip β for model 3 with 0- and $2\frac{7}{16}$ - inch gap size. End plate 5; driving vane on; q = 8.

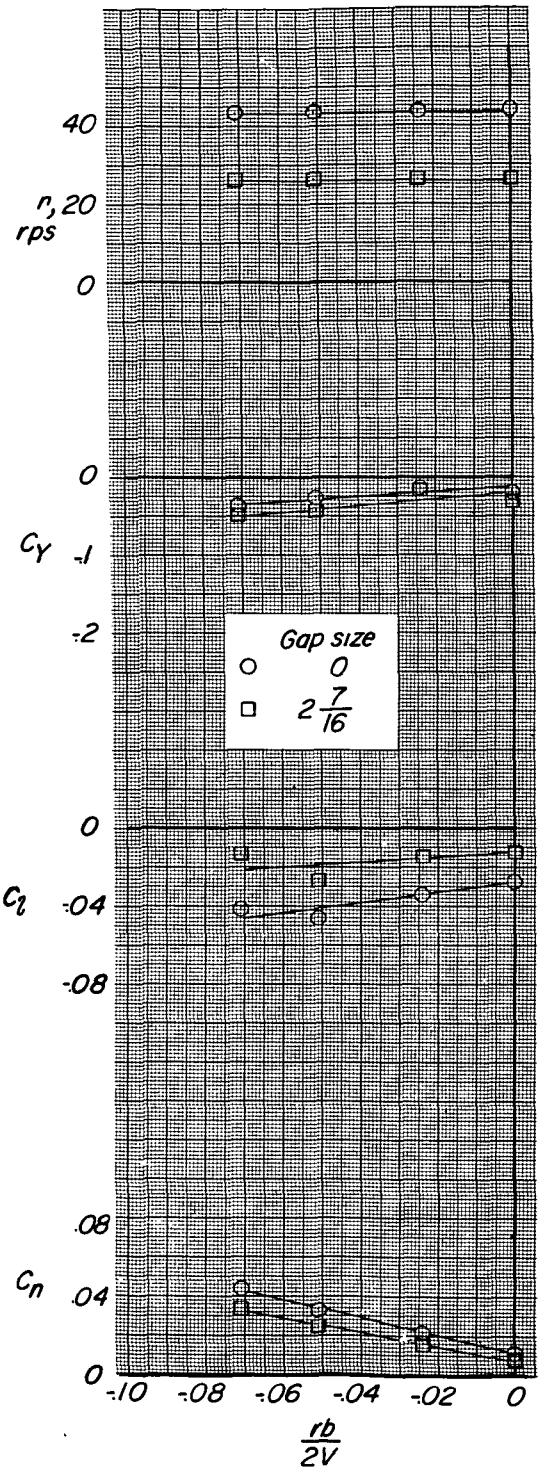

Figure 33.- Variation of C_n, C_l, C_Y, and n with rb/2V for model 3 with 0- and $2\frac{7}{16}$-inch gap size. End plate 5; driving vane on; q = 8.

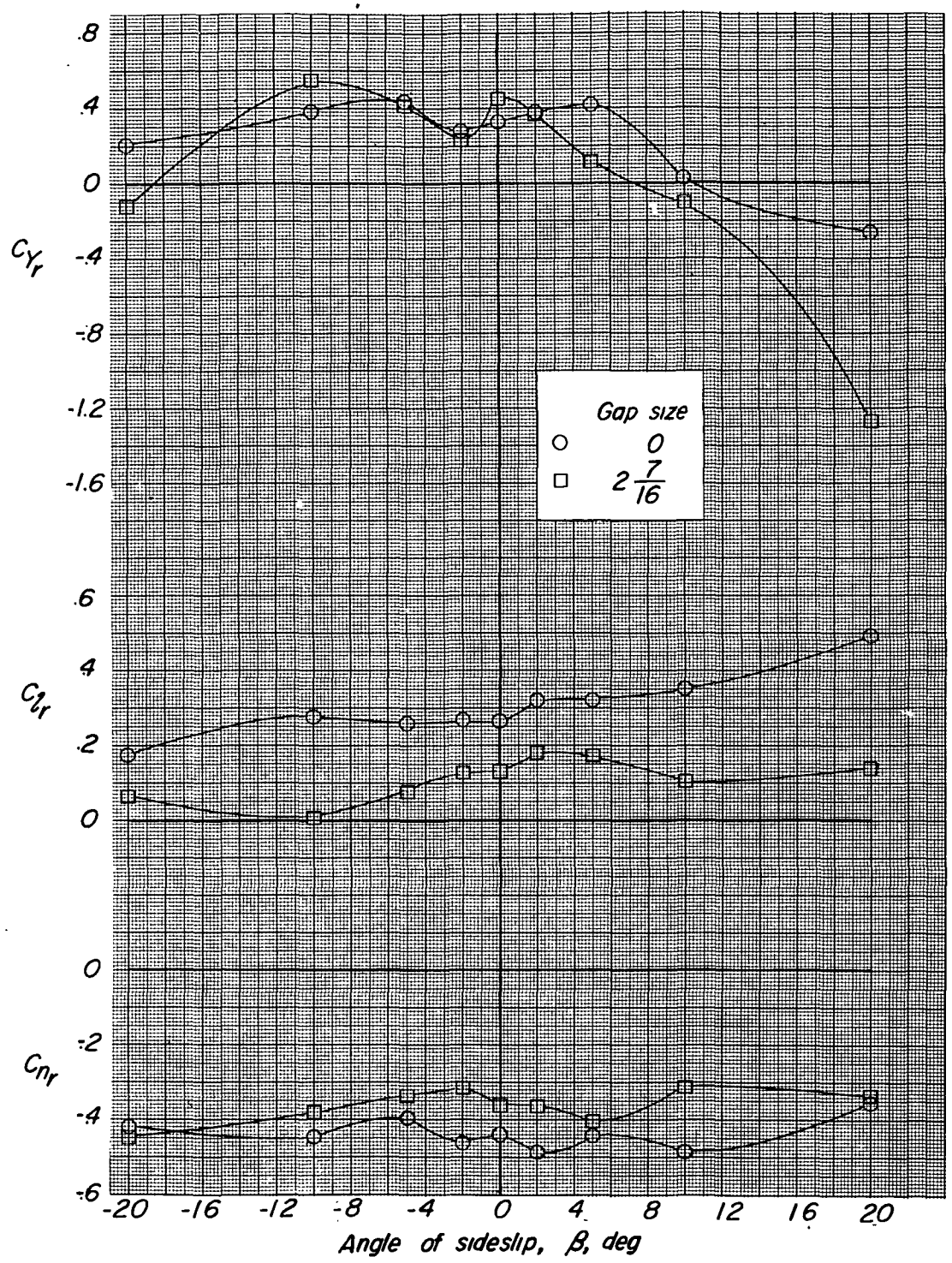

Figure 34.- Variation of C_{n_r}, C_{l_r}, and C_{Y_r} with angle of sideslip β for model 3 with 0- and $2\frac{7}{16}$-inch gap size. End plate 5; driving vane on; q = 8.

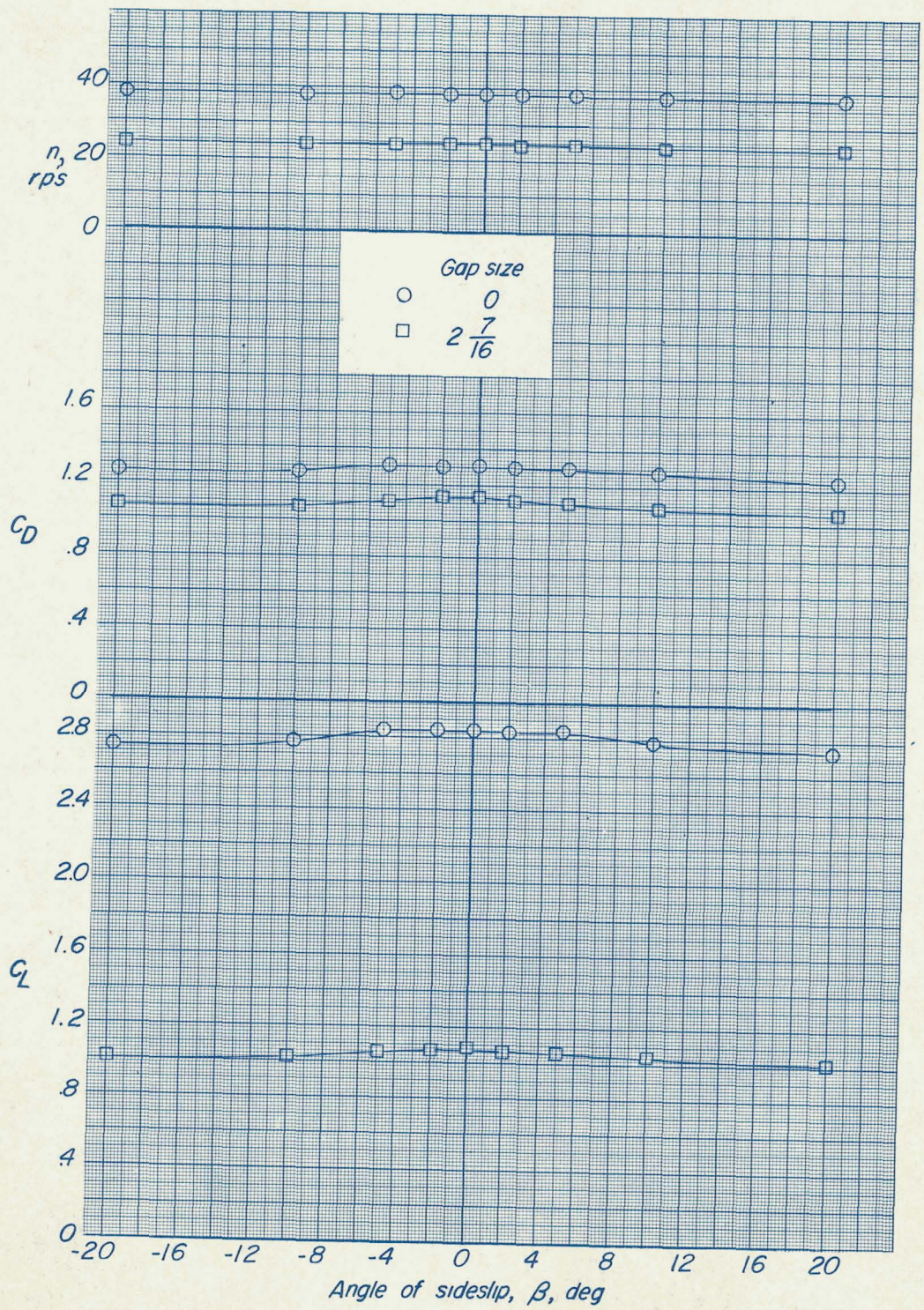

Figure 35.- Variation of C_L, C_D, and n with angle of sideslip β for model 3 with 0- and $2\frac{7}{16}$ - inch gap size. End plate 6; driving vane on; q = 8.

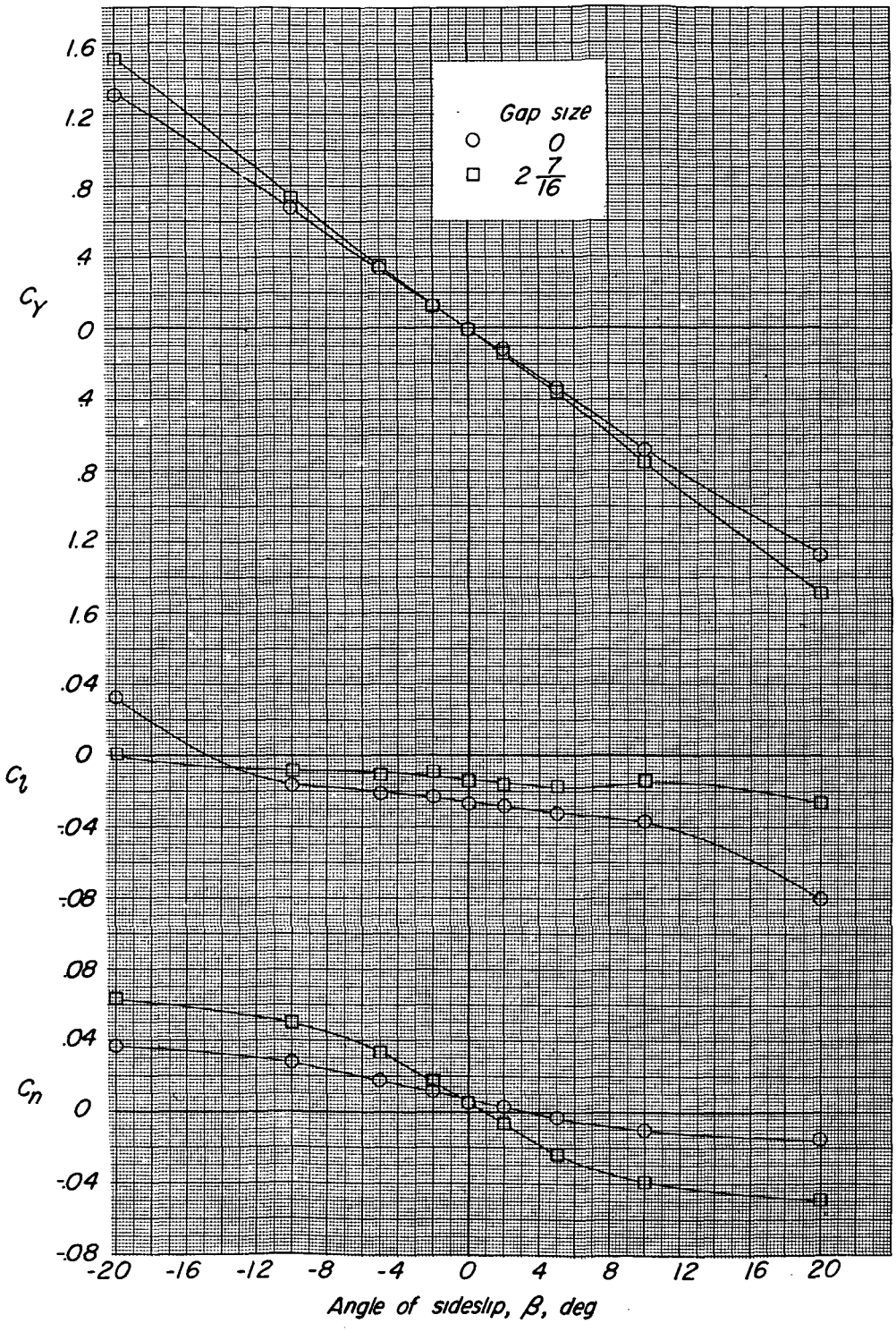

Figure 36.- Variation of C_n, C_l, and C_Y with angle of sideslip β for model 3 with 0- and $2\frac{7}{16}$-inch gap size. End plate 6; driving vane on; q = 8.

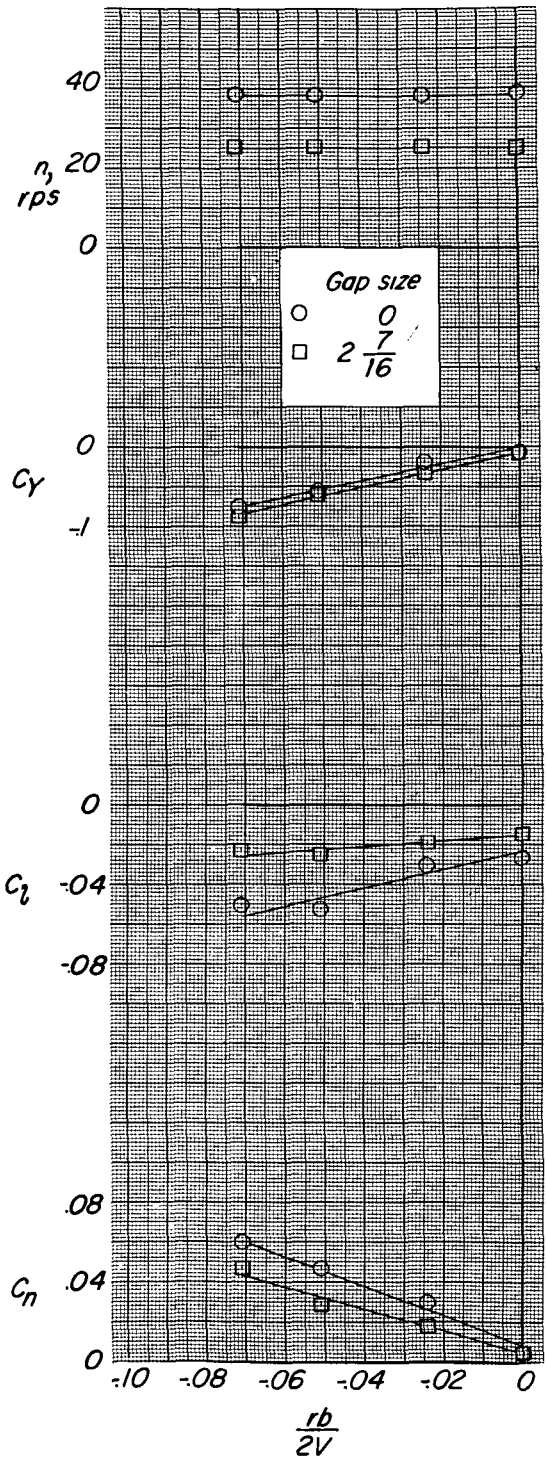

Figure 37.- Variation of C_n, C_l, C_Y, and n with rb/2V for model 3 with 0- and $2\frac{7}{16}$-inch gap size. End plate 6; driving vane on; q = 8.

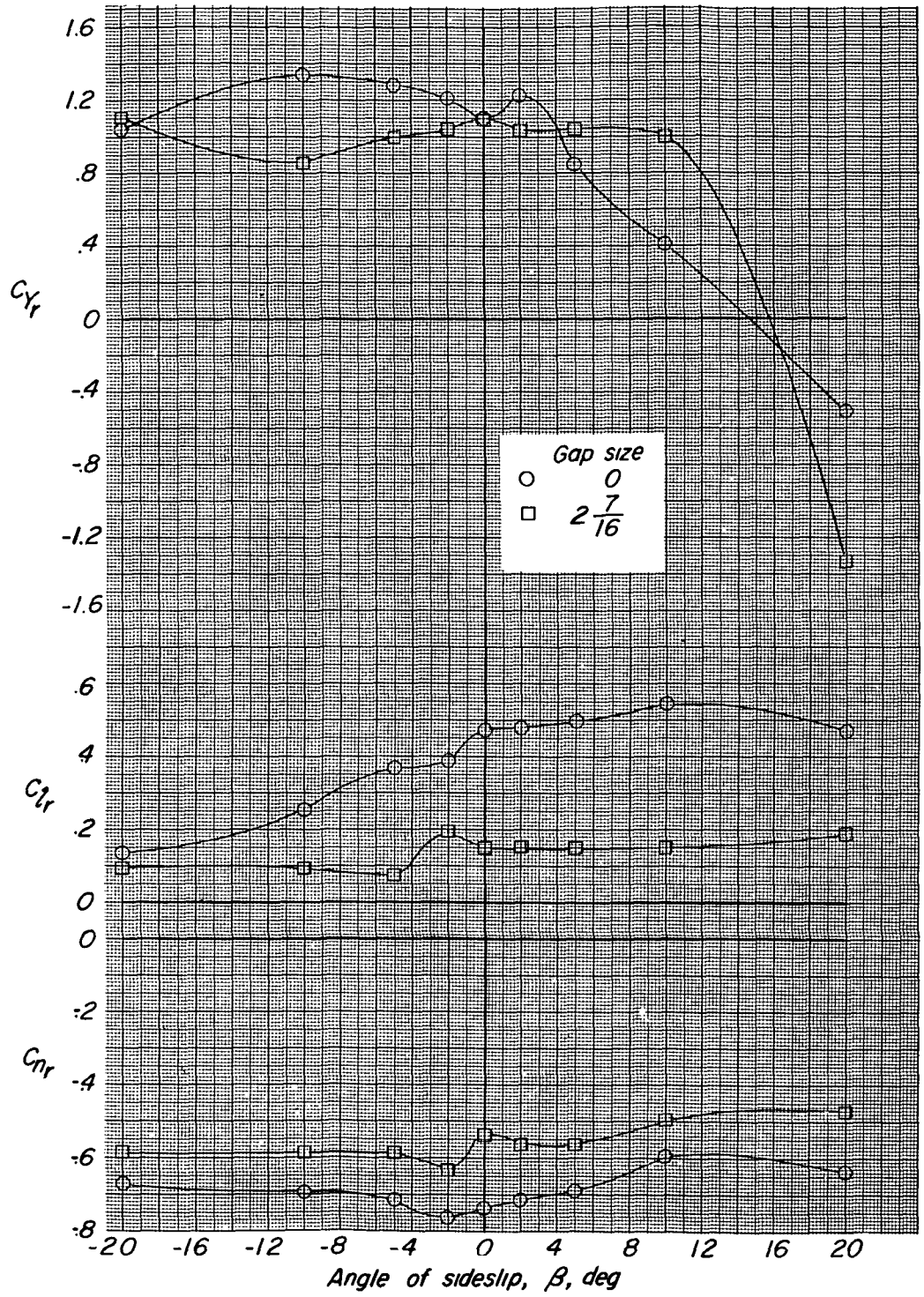

Figure 38.- Variation of C_{n_r}, C_{l_r}, and C_{Y_r} with angle of sideslip β for model 3 with 0- and $2\frac{7}{16}$-inch gap size. End plate 6; driving vane on; $q = 8$.

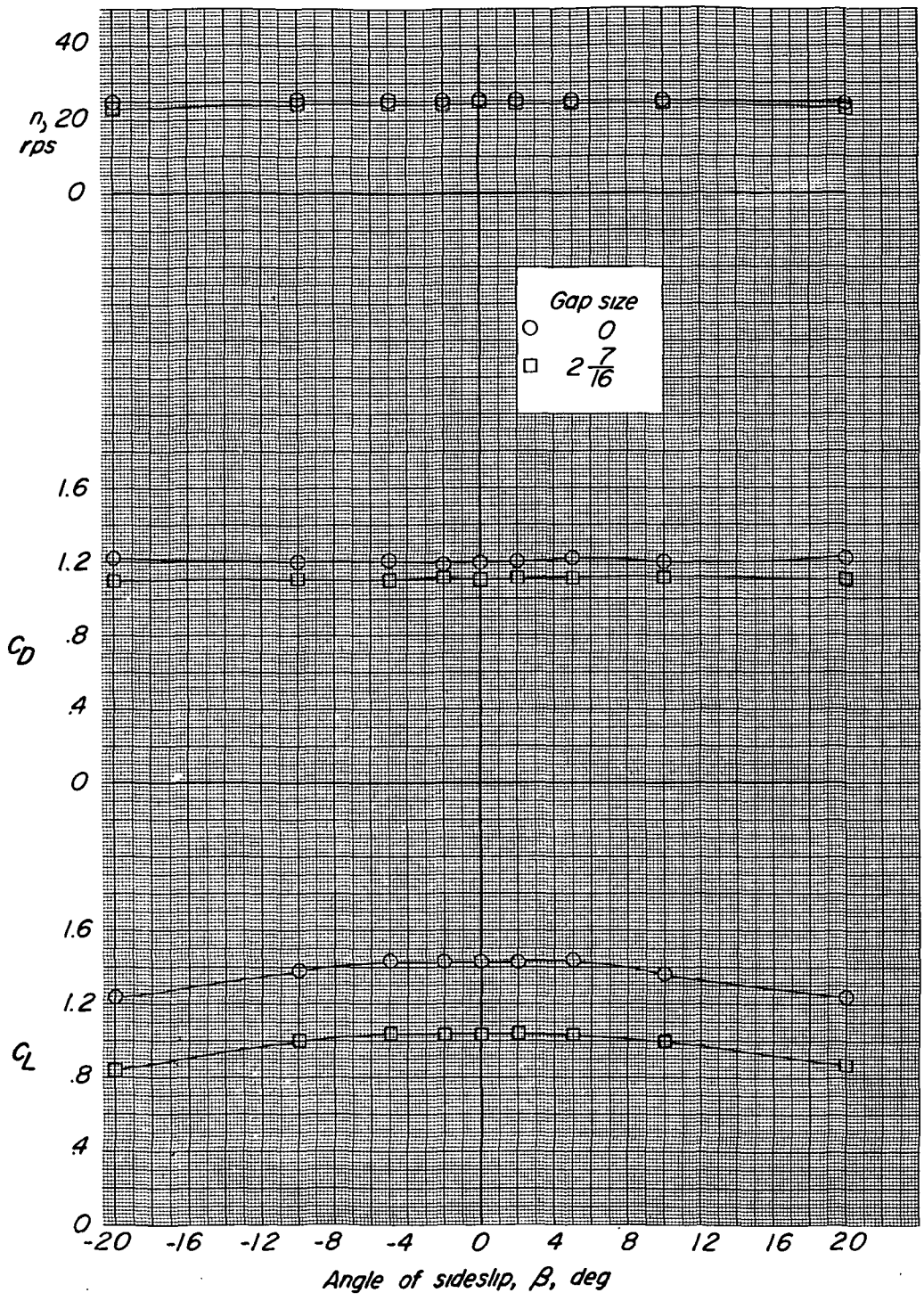

Figure 39.- Variation of C_L, C_D, and n with angle of sideslip β for model 3 with 0- and $2\frac{7}{16}$-inch gap size. End plate 7; driving vane on; q = 8.

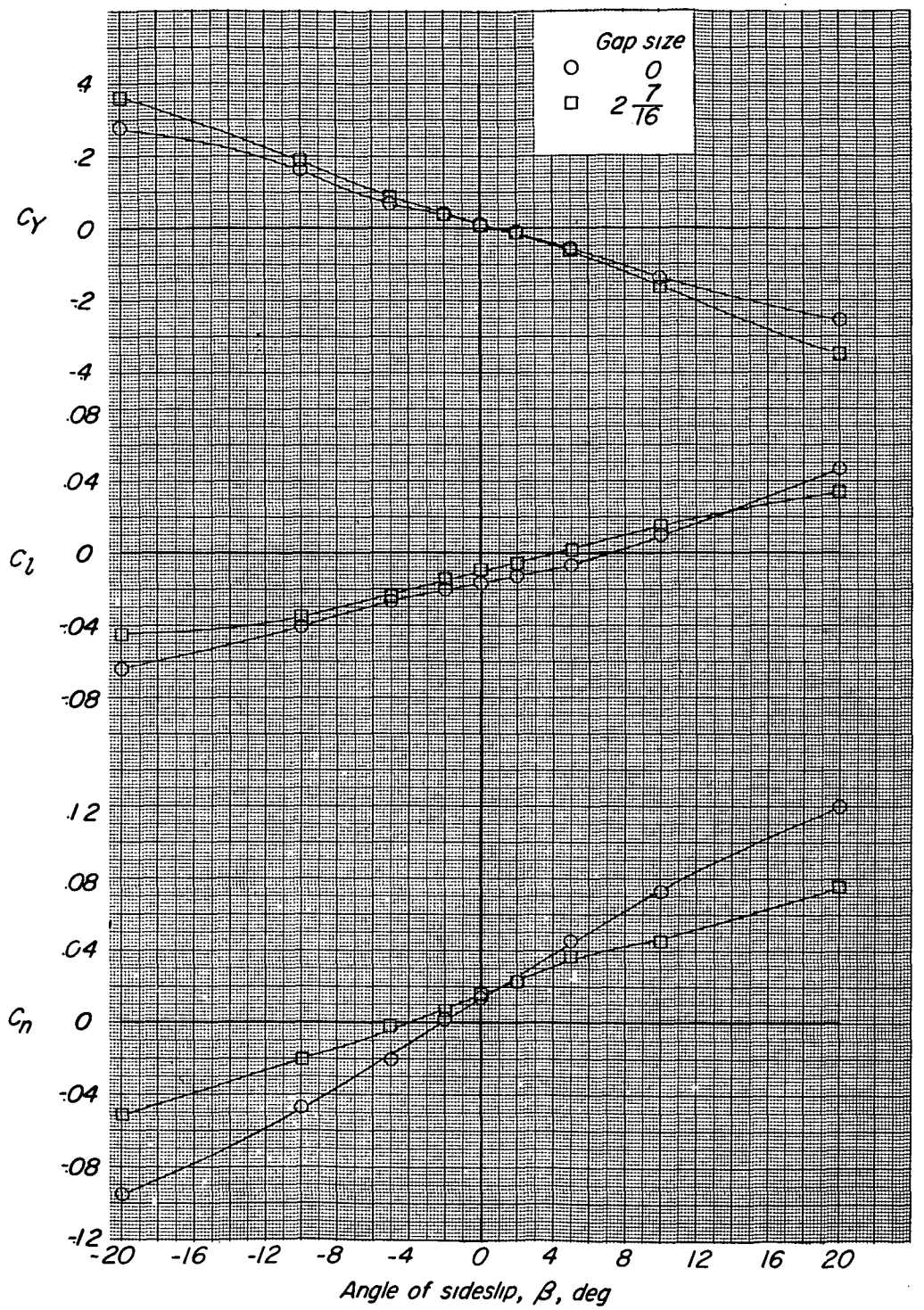

Figure 40.- Variation of C_n, C_l, and C_Y with angle of sideslip β for model 3 with 0- and $2\frac{7}{16}$-inch gap size. End plate 7; driving vane on; $q = 8$.

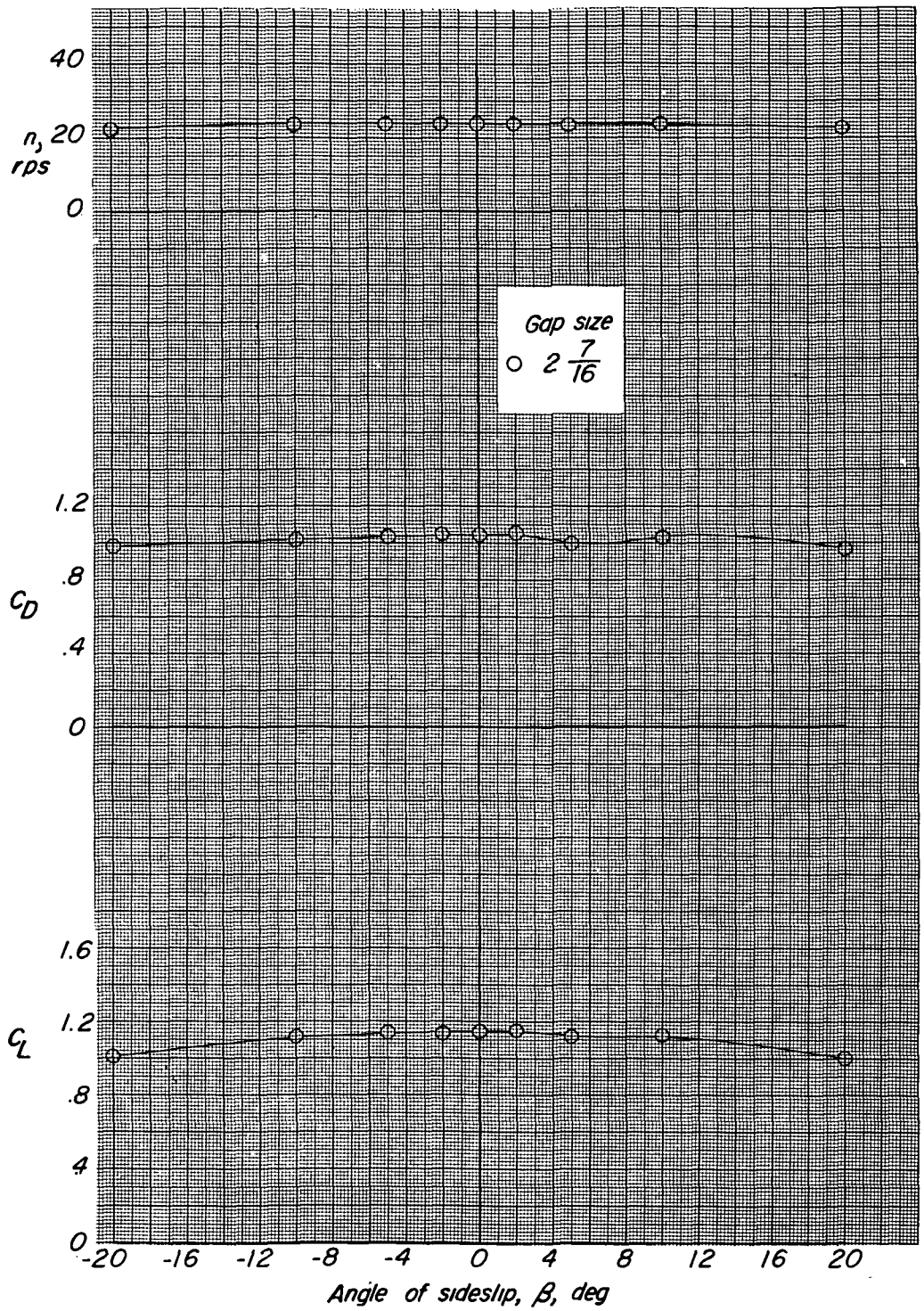

Figure 41.- Variation of C_L, C_D, and n with angle of sideslip β for model 3 with $2\frac{7}{16}$- inch gap size. End plate 1; driving vane off; q = 8.

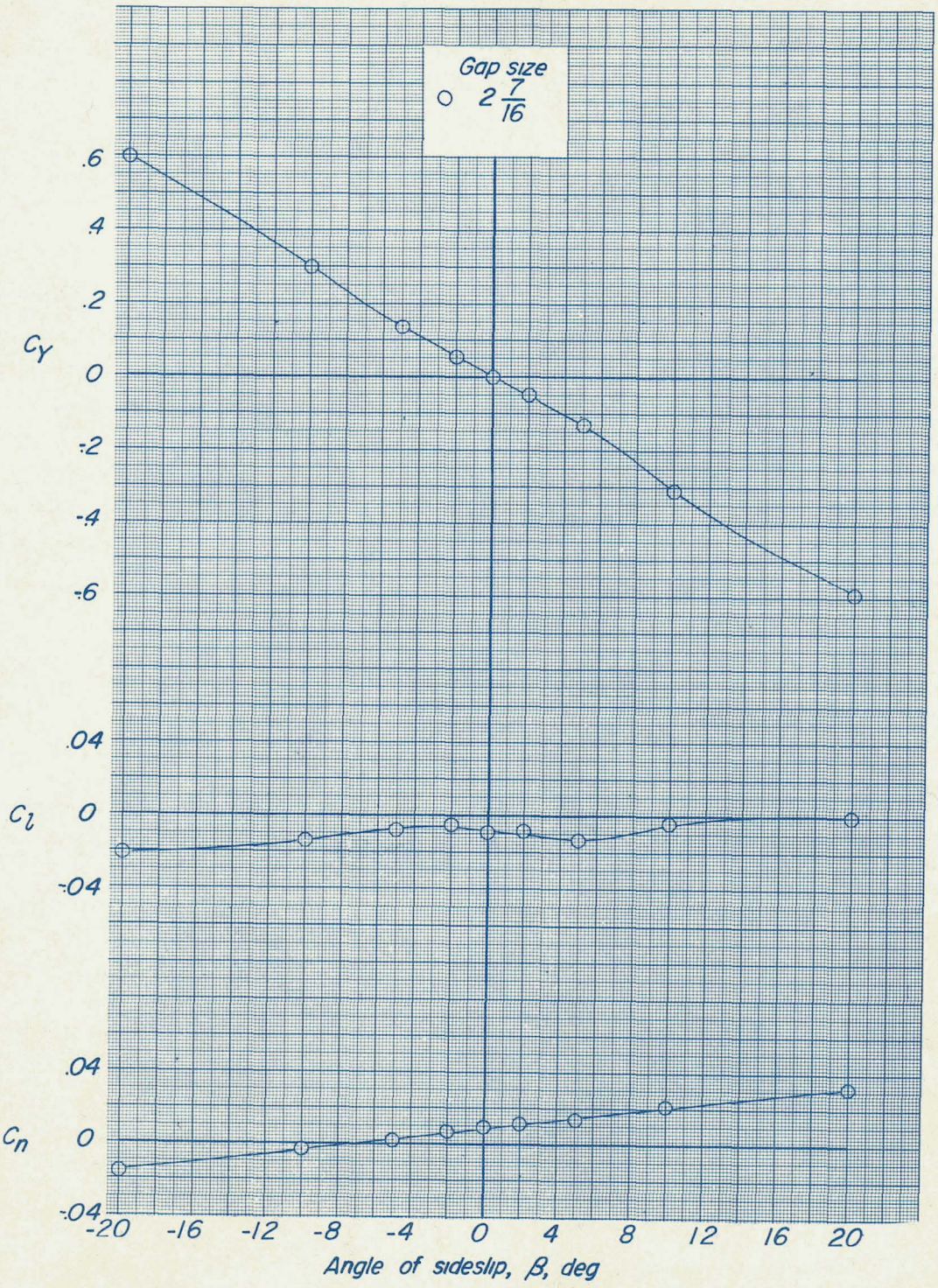

Figure 42.- Variation of C_n, C_l, and C_Y with angle of sideslip β for model 3 with $2\frac{7}{16}$-inch gap size. End plate 1; driving vane off; q = 8.

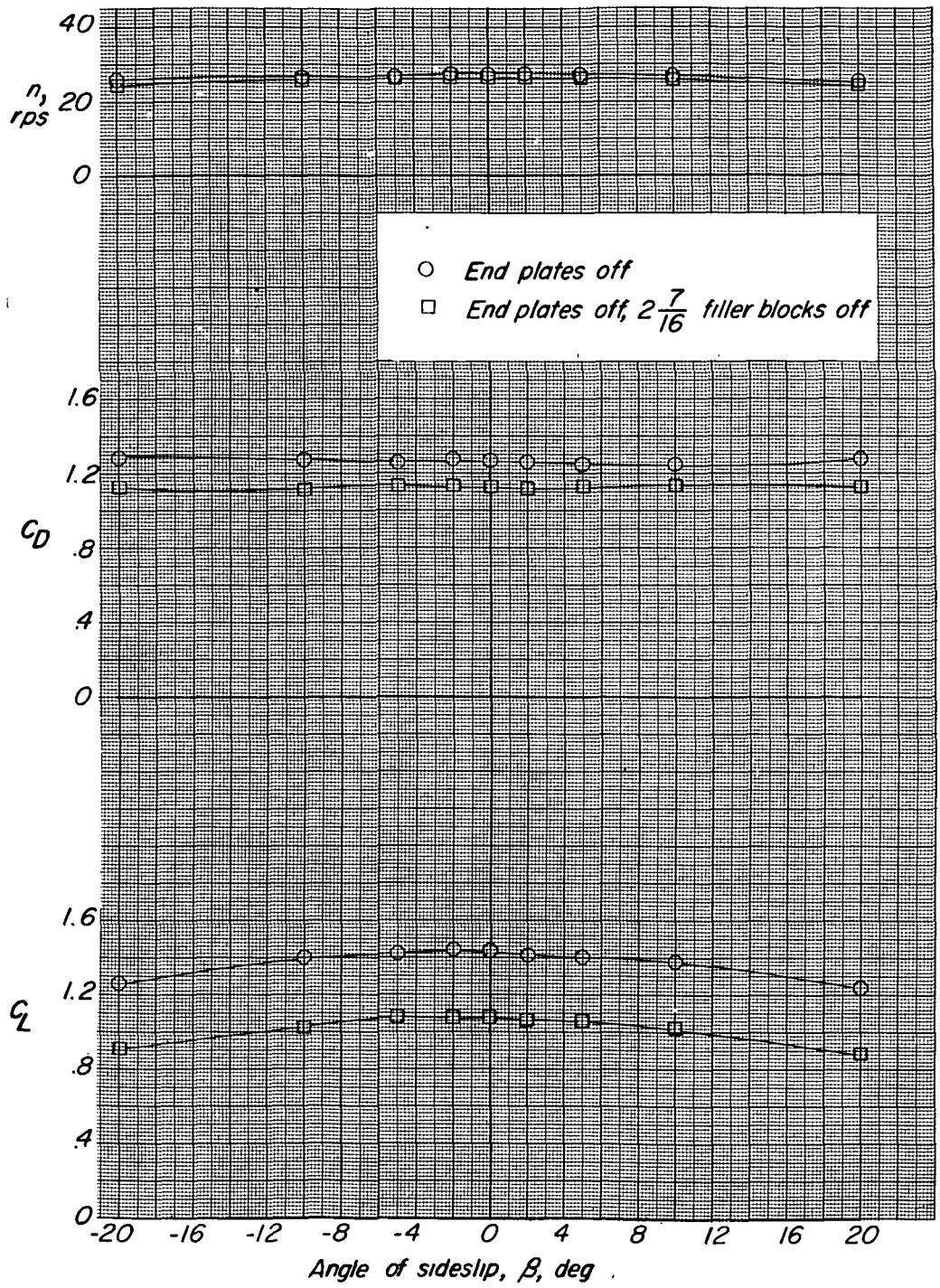

Figure 43.- Variation of C_L, C_D, and n with angle of sideslip β for model 3 with end plates off and with end plates and $2\frac{7}{16}$-inch filler blocks off. Driving vane on; q = 8.

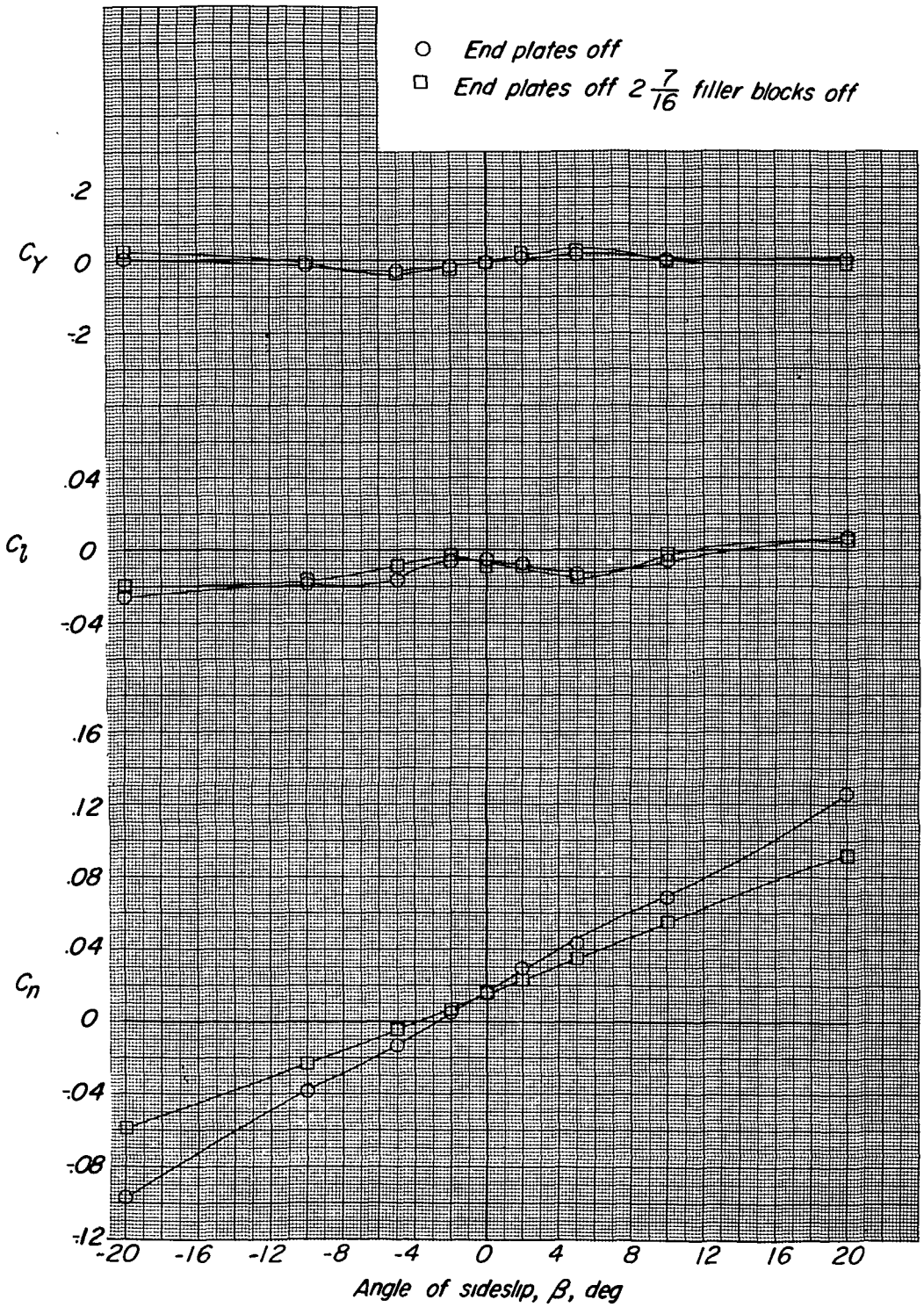

Figure 44.- Variation of C_n, C_l, and C_Y with angle of sideslip β for model 3 with end plates off and with end plates and $2\frac{7}{16}$-inch filler blocks off. Driving vane on; $q = 8$.

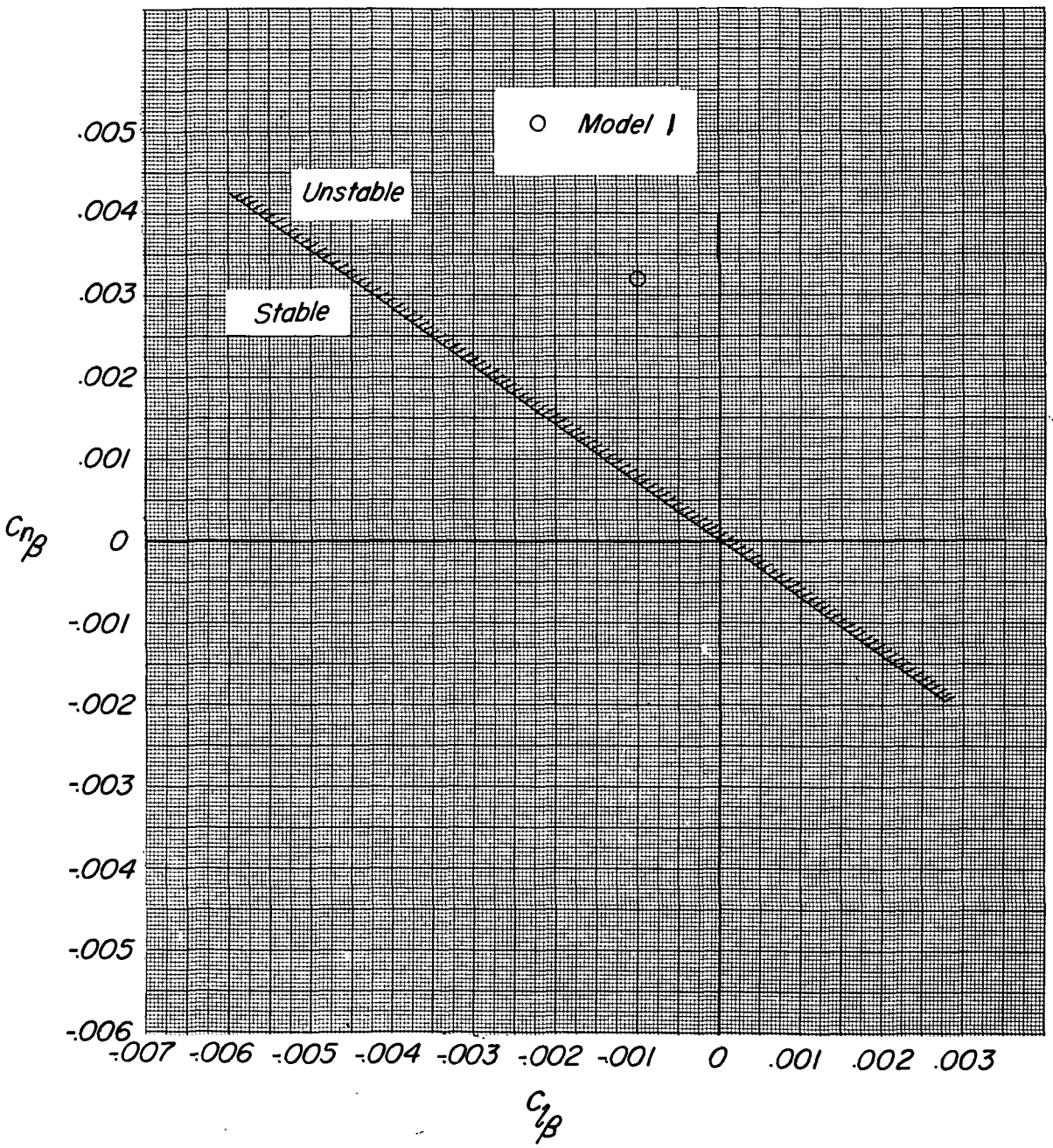

Figure 45.- Spiral stability boundary for model 1 with position of model 1 with respect to the boundary. q = 8.

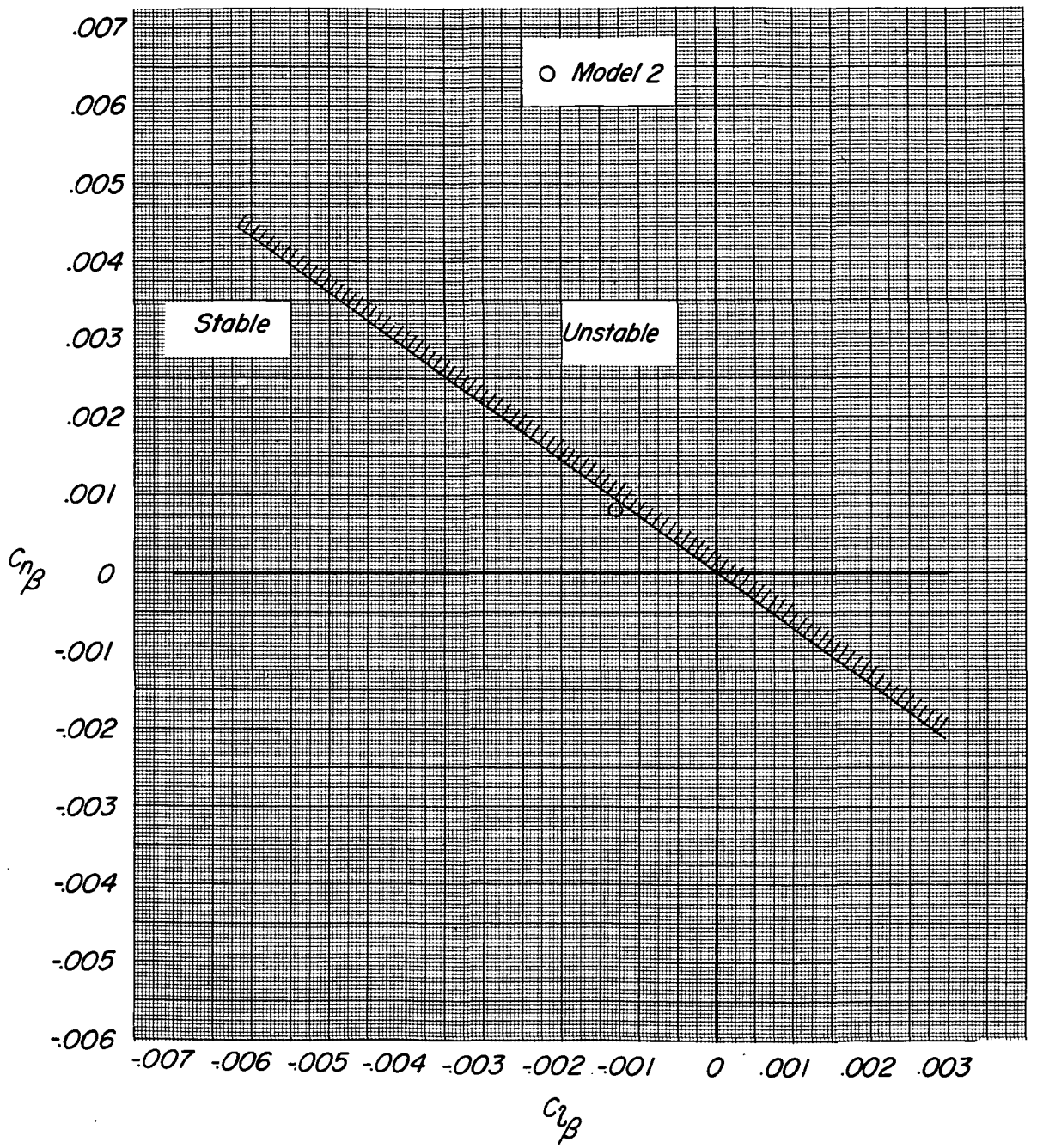

Figure 46.- Spiral stability boundary for model 2 with position of model 2 with respect to the boundary. q = 16.

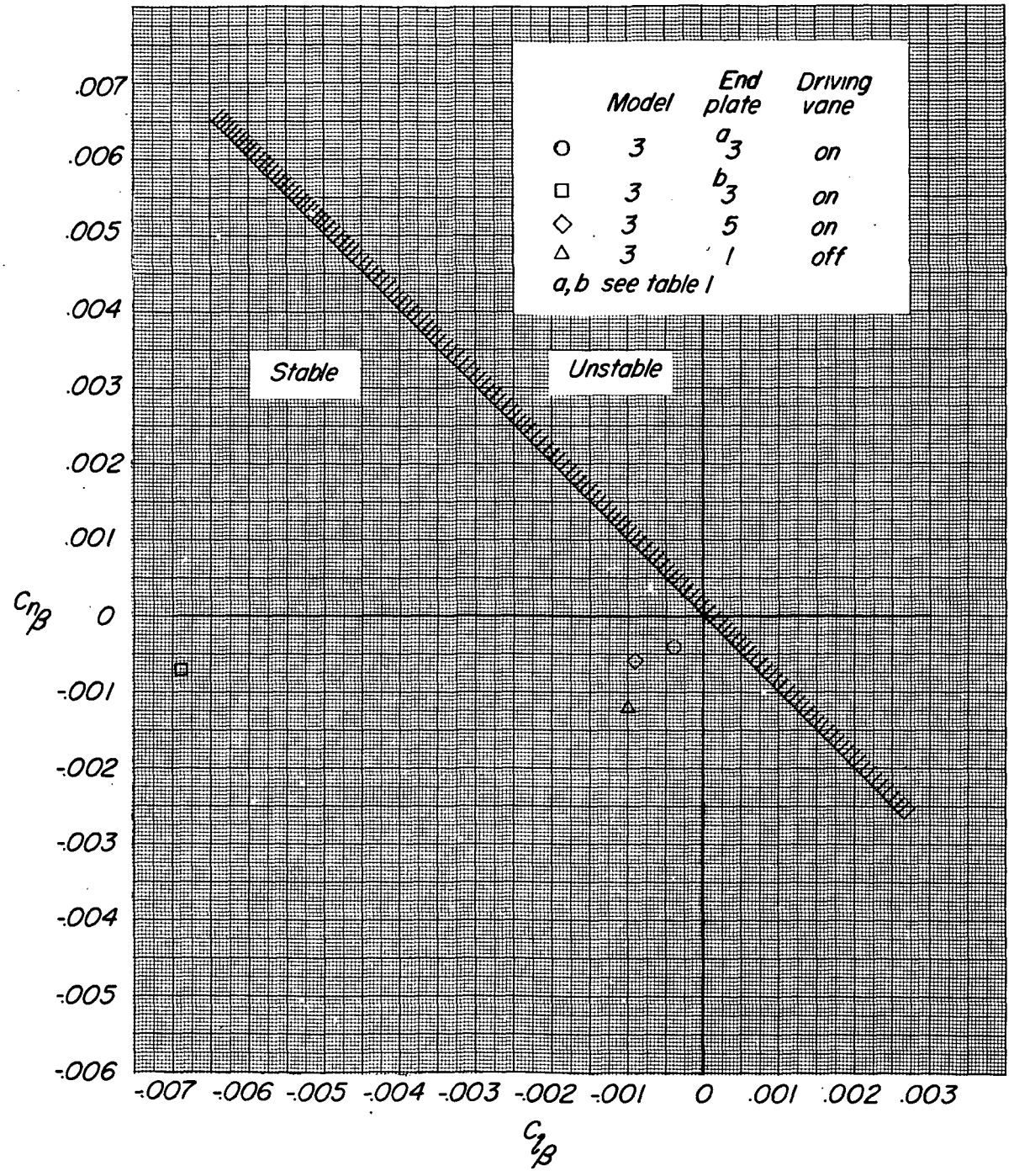

Figure 47.- Spiral stability boundary for several models and position of models with respect to the boundary. q = 8.